This version of the ESI published 09/02/2022 replaces the previous version published 25/09/2019. Formula $EAPbBr_3$ is replaced with the correct version EA_2PbBr_4 throughout.

Electronic Supplementary Information

Hybrid blue perovskite@metal-organic gel (MOG) nanocomposite: dramatic improvement of luminescence property and stability

Samraj Mollick,[a†] Tarak Nath Mandal,[a†] Atanu Jana,[b] Sahel Fajal[a] and Sujit K. Ghosh*[ac]

[a]Department of Chemistry, Indian Institute of Science Education and Research (IISER), Dr. Homi Bhabha Road, Pashan, Pune 411008, India.

[b]Center for Super functional Materials, Department of Chemistry, School of Natural Science, Ulsan National Institute of Science and Technology (UNIST), Ulsan 44919, South Korea.

[c]Centre for Energy Science, IISER Pune, Pune 411008, India.

[†]These authors contributed equally to this work.

Corresponding author. E-mail: sghosh@iiserpune.ac.in

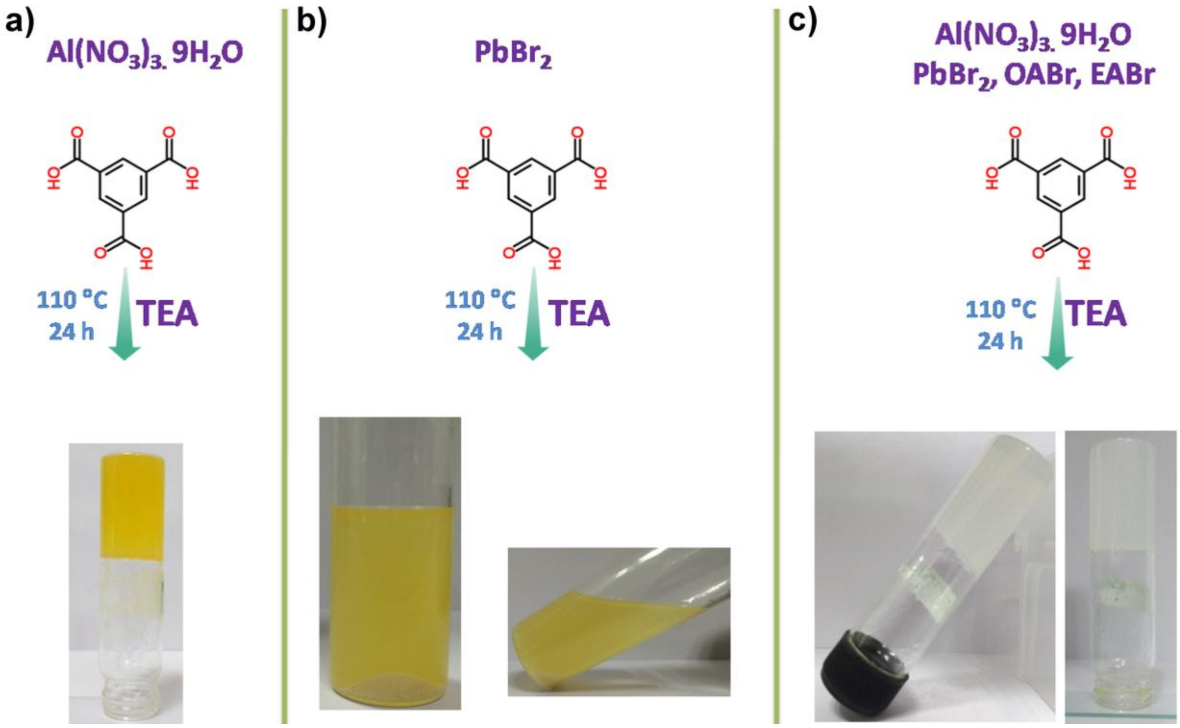

Figure S1. Synthesis of MOG presence of different metal ions and reactants.
a) MOG formed with Al(III) metal ions. b) MOG was not formed with Pb(II) metal ions. c) MOG was formed presence perovskite precursors. TEA represent triethylamine base.

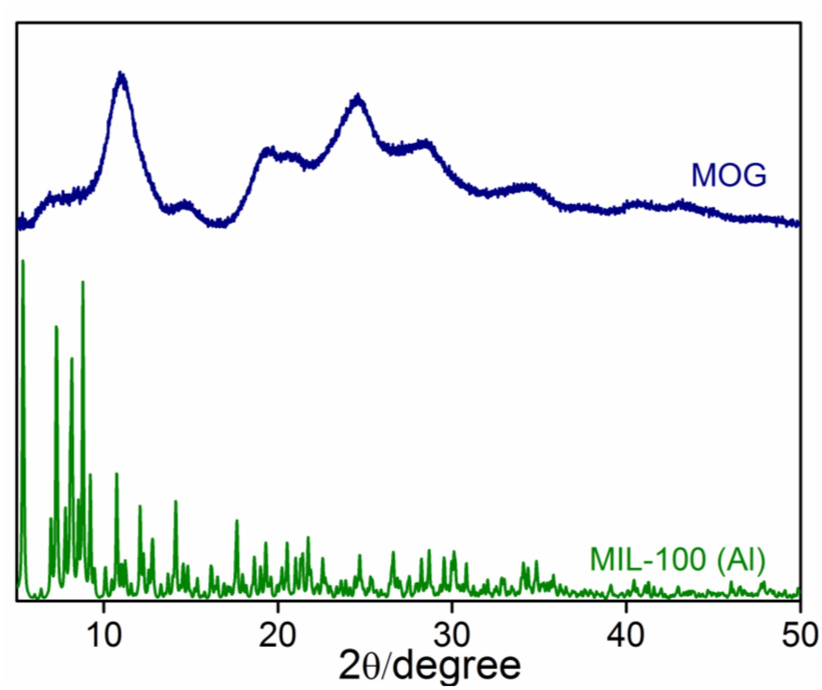

Figure S2. Comparison of PXRD patterns of MIL-100 (Al) and metal-organic gal (MOG).

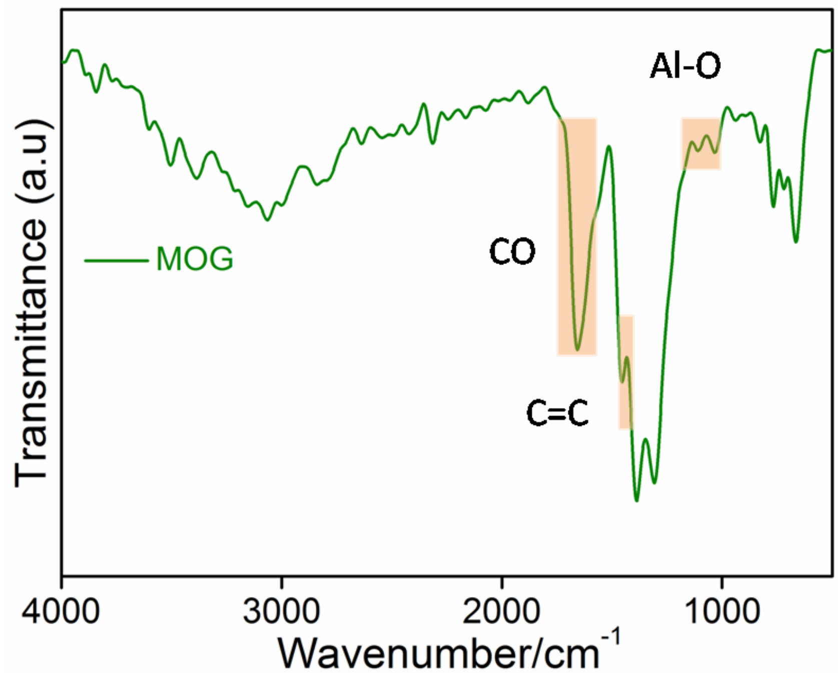

Figure S3. FT-IR spectra of pristine MOG. Highlighted peak indicates the characteristics peaks of MOG host matrix.

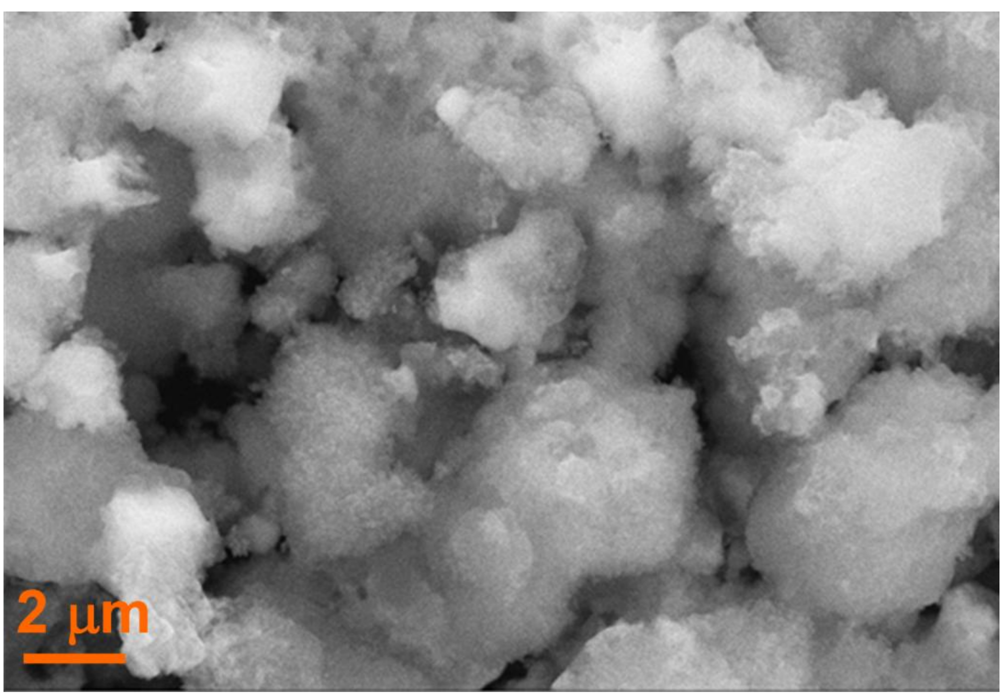

Figure S4. FESEM image of pristine MOG. The pristine MOG has sponge type morphology.

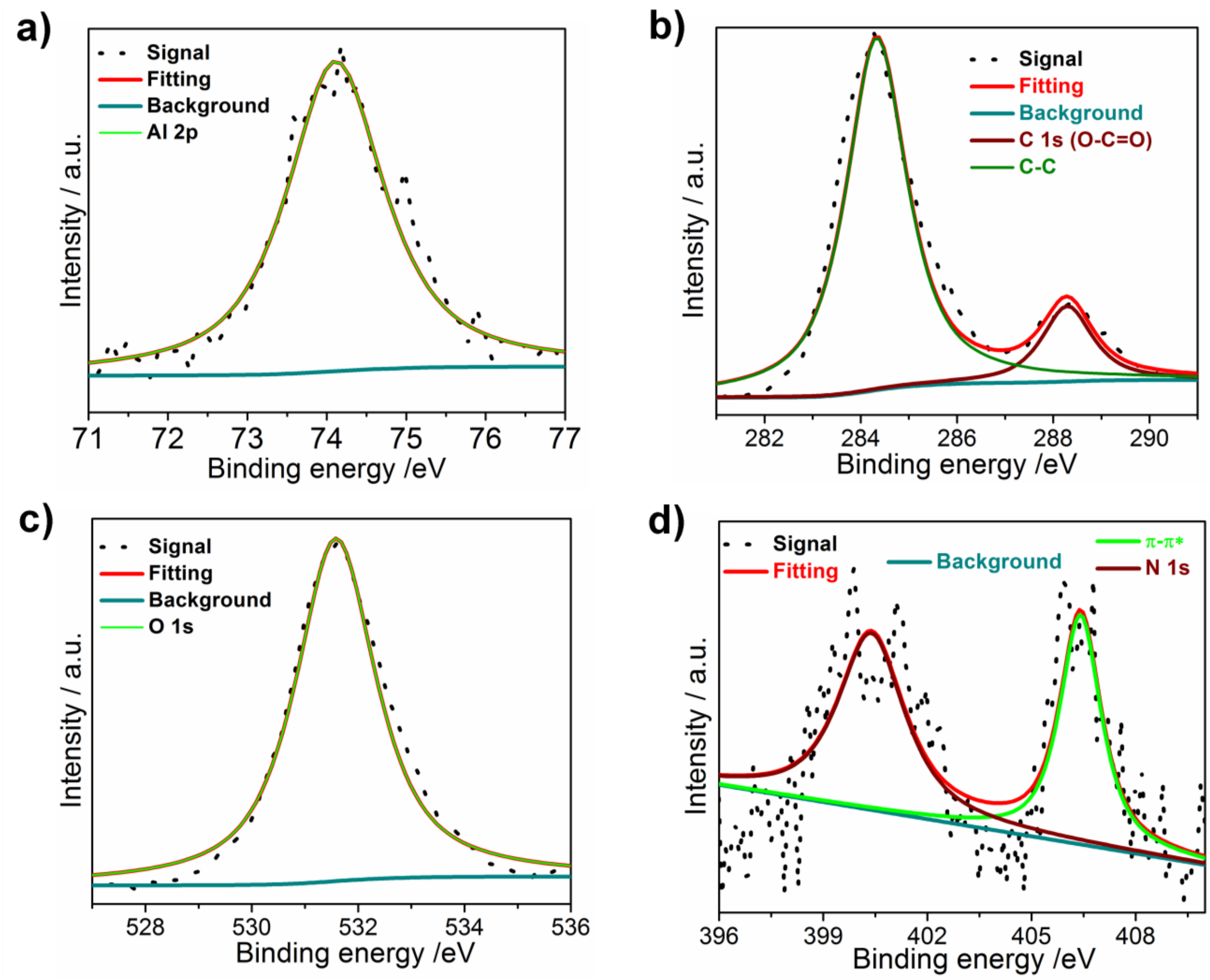

Figure S5. XPS spectra of MOG. (a) Al 2p; (b) C 1s (O-C=O) and C-C; (c) O 1s; (d) N 1s and π-π*.

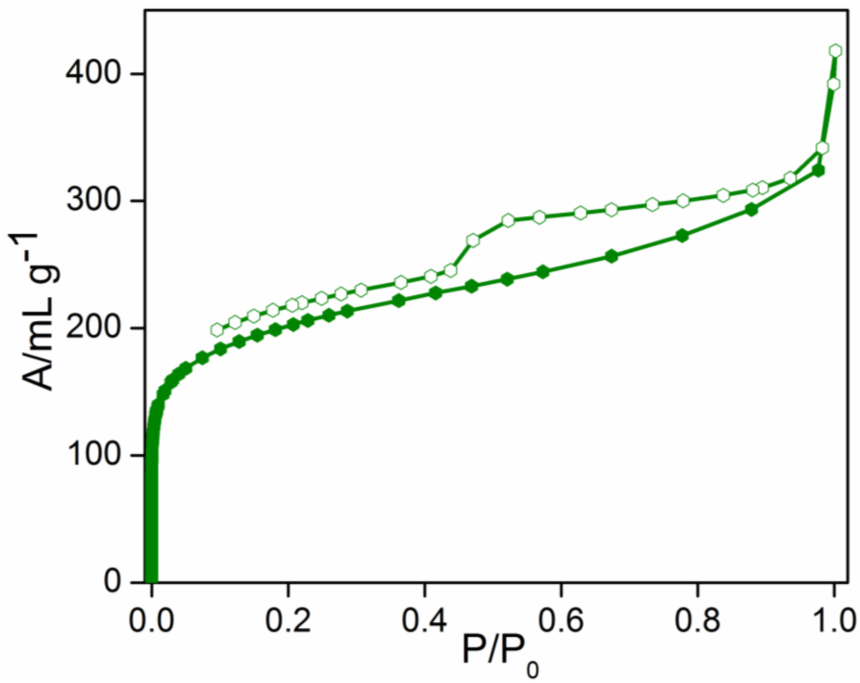

Figure S6. N_2 sorption study at 77 K for pristine MOG.

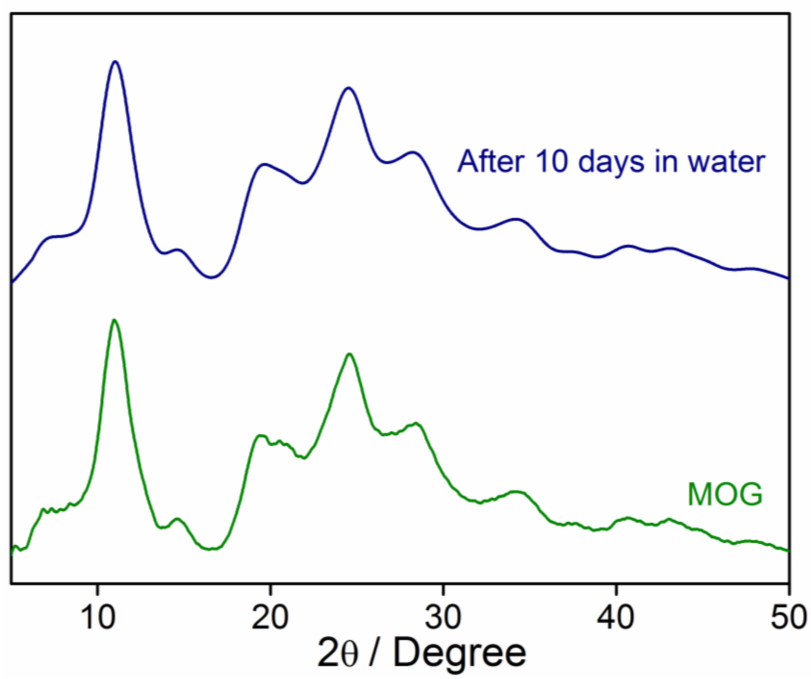

Figure S7. PXRD patterns for confirmation of water stability of pristine MOG.

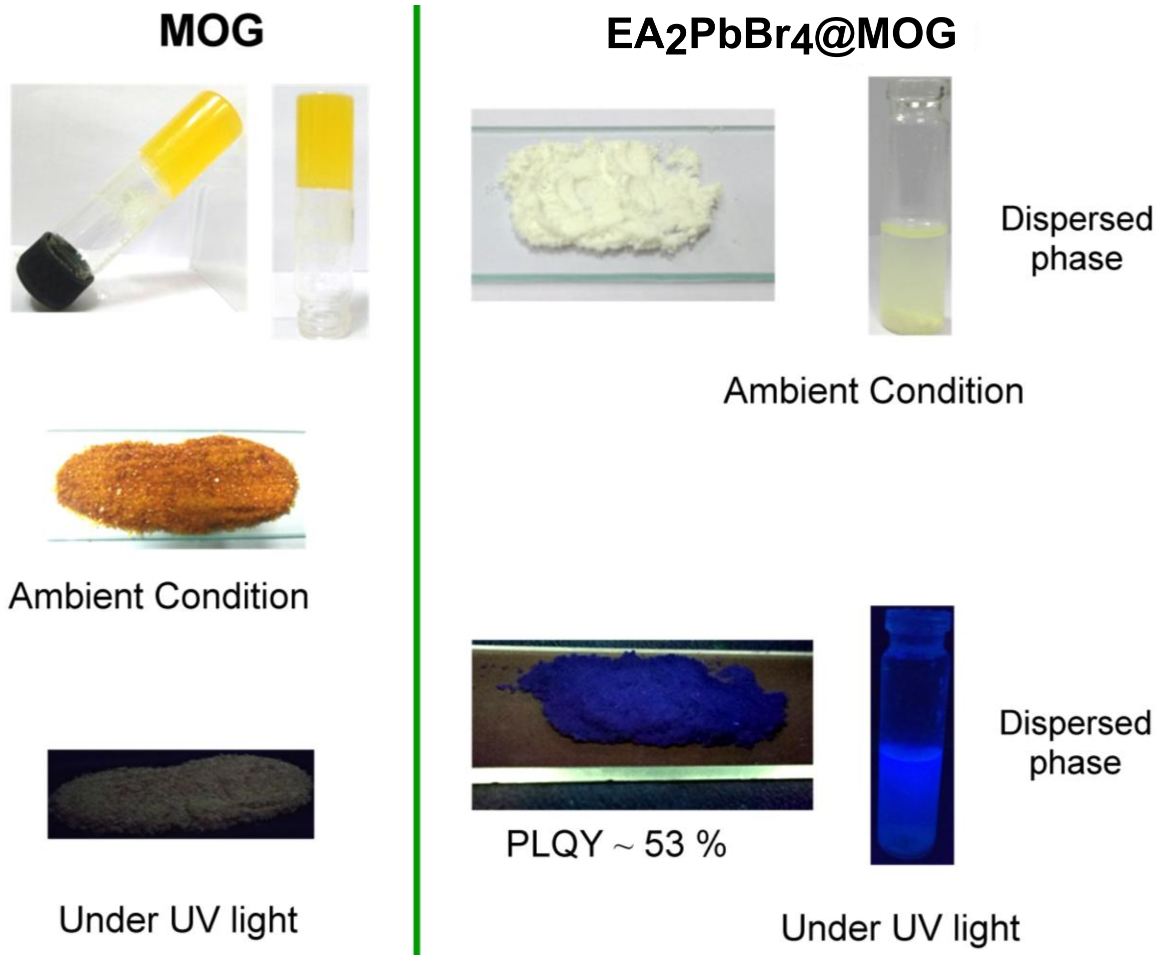

Figure S8. Photographs of Pristine MOG and EA_2PbBr_4@MOG at ambient conditions and under UV light (365 nm). Toluene solvent was used for dispersion of EA_2PbBr_4@MOG composite.

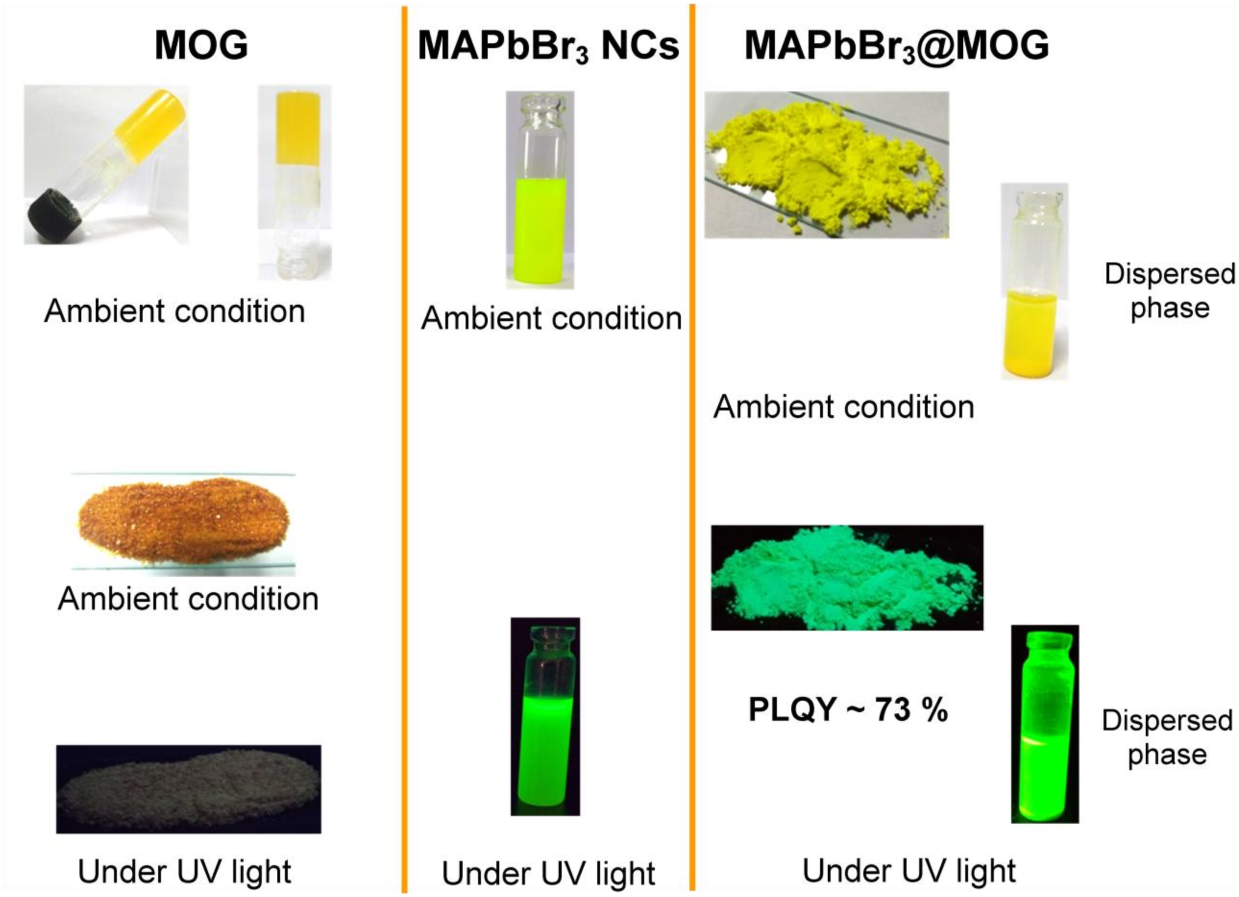

Figure S9. Photographs of Pristine MOG and $MAPbBr_3$ NCs and $MAPbBr_3$@MOG at ambient conditions and under UV light (365 nm). Toluene solvent was used for dispersion of $MAPbBr_3$@MOG composite.

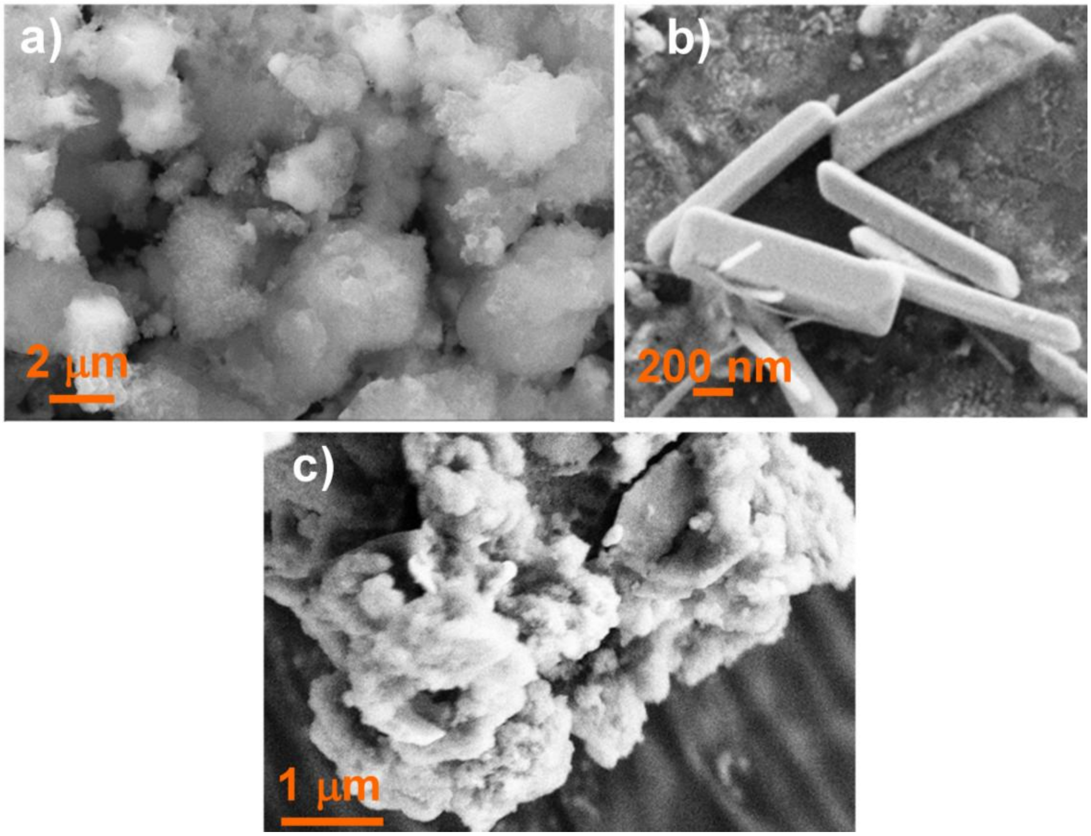

Figure S10. FESEM image. a) MOG, b) EA_2PbBr_4 NCs and c) EA_2PbBr_4@MOG composite.

Table S1. EDX analysis from FESEM experiment of EA_2PbBr_4@MOG composite.

Element	Weight %	Atomic %
C K	36.34	59.37
O K	20.18	24.75
N K	4.63	5.31
Al K	4.76	3.46
Br L	17.86	5.57
Pb M	16.23	1.54
Total	100.00	100.00

Table S2. Pb/Br ratio of $MAPbBr_3$@ZIF-8 composite is 3.62. Higher ratio of Br than Pb indicates the formation of EA_2PbBr_4 perovskite NPs in composite material.

Element	Molar Ratio
Pb	1.54
Br	5.57

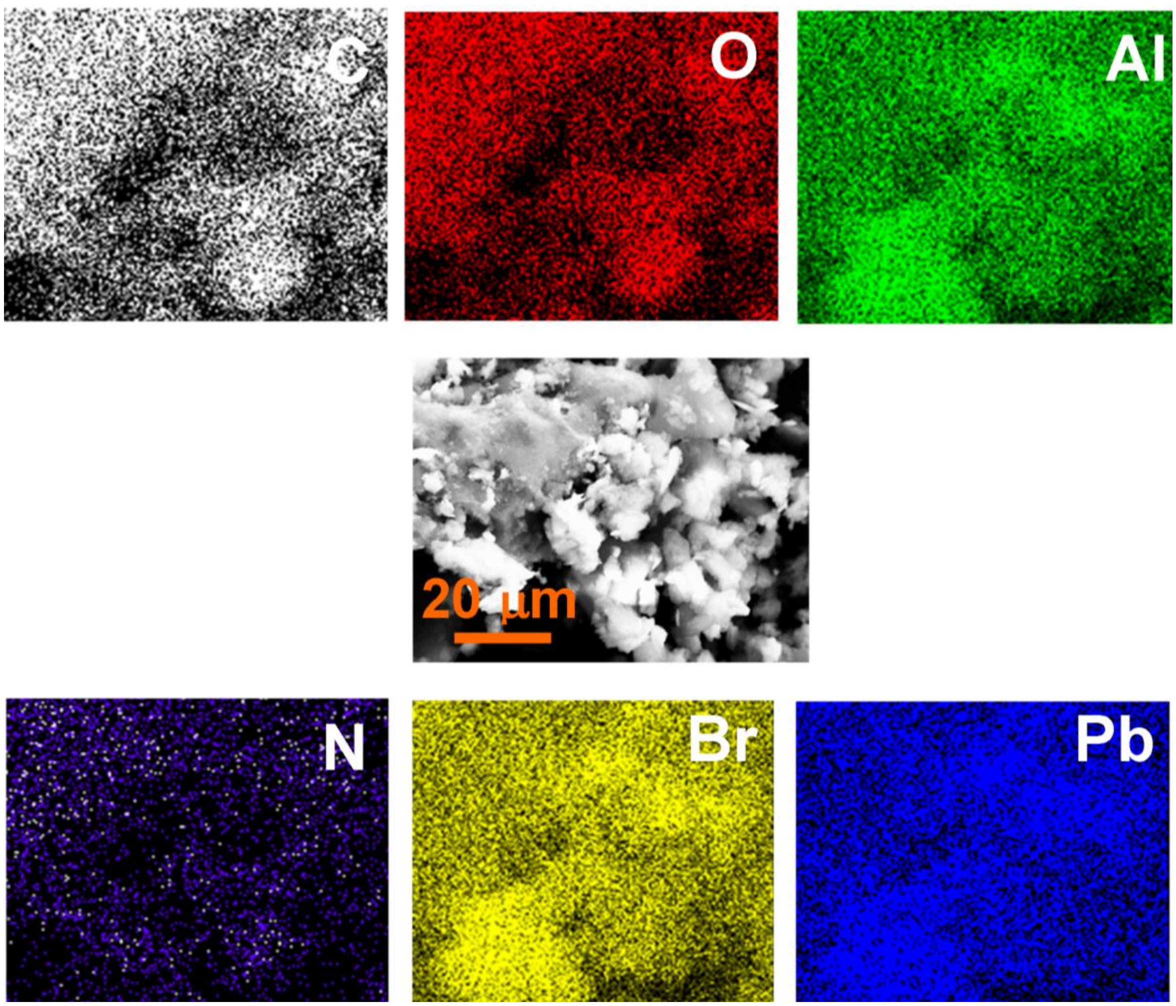

Figure S11. Elemental mapping of EA_2PbBr_4@MOG composite. Elemental mapping analysis shows that Pb and Br are present throughout the composite which indicates the homogeneous formation of perovskite NCs in composite.

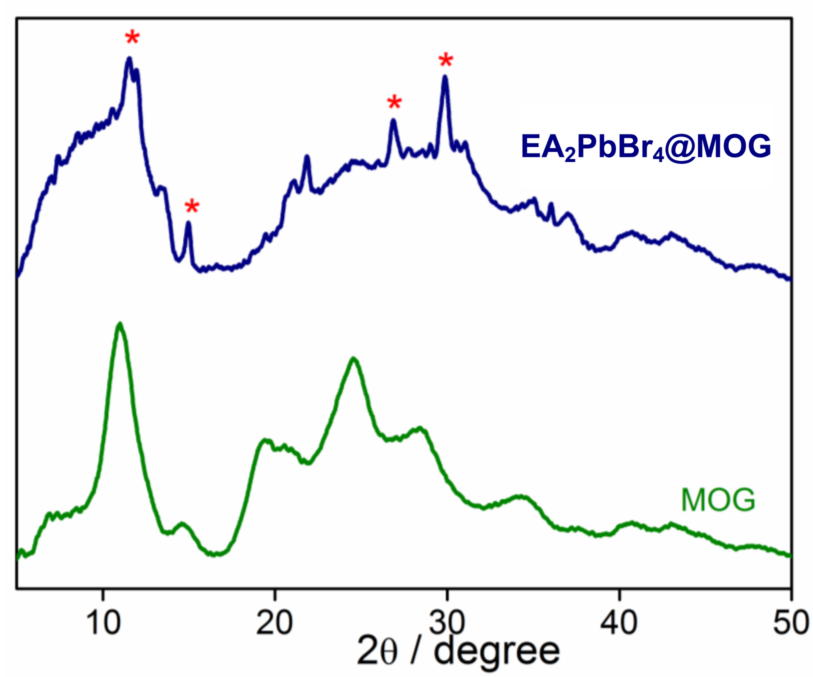

Figure S12. PXRD patterns of MOG and EA_2PbBr_4@MOG composite. Star represent the peak position of EA_2PbBr_4 NPs, representing formation of EA_2PbBr_4 NCs in composite material.

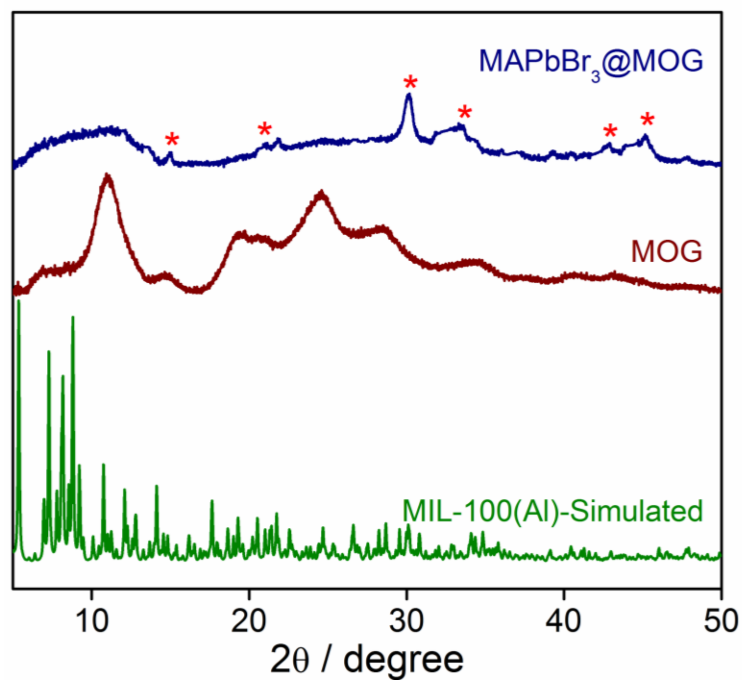

Figure S13. Comparison of PXRD patterns of MIL-101 (Al), MOG and $MAPbBr_3$@MOG composite. Star represent the peak position of $MAPbBr_3$ NCs, indicating formation of $MAPbBr_3$ NCs in composite material.

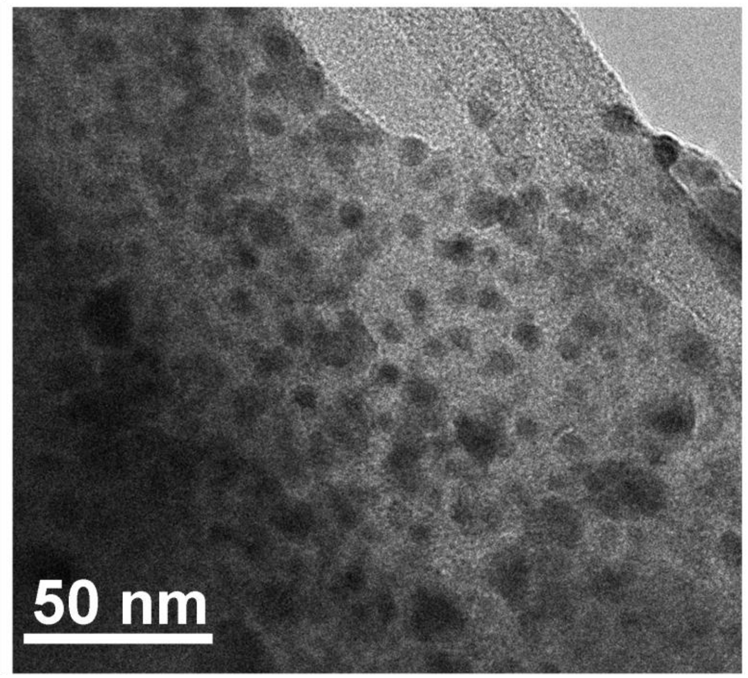

Figure S14. Large area TEM image EA_2PbBr_4@ MOG nanocomposite.

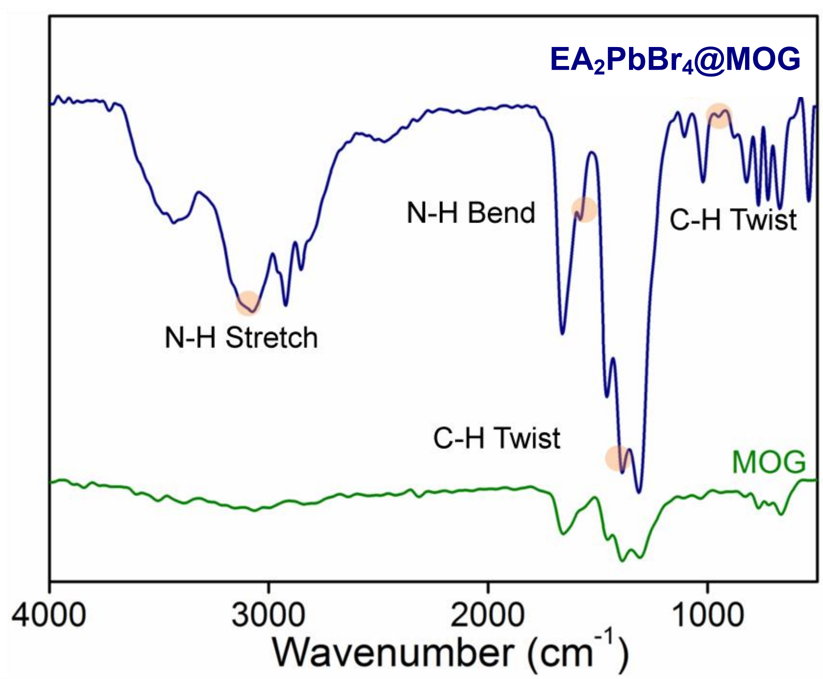

Figure S15. FT-IR spectra of MOG and EA_2PbBr_4@MOG. Highlighted peaks indicate the characteristic peaks for EA_2PbBr_4 perovskite material, representing formation of EA_2PbBr_4 NCs in composite material.

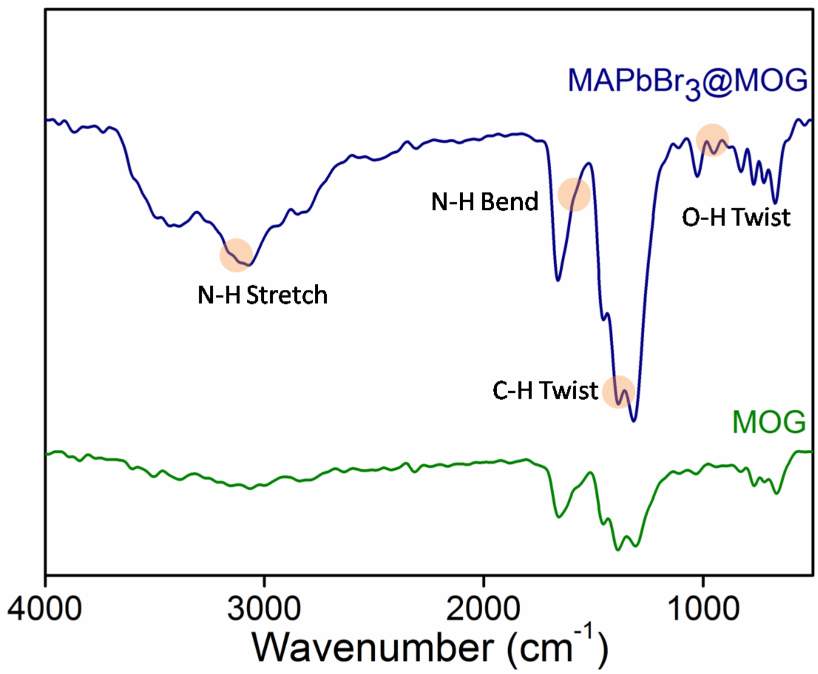

Figure S16. FT-IR spectra of MOG and $MAPbBr_3$@MOG. Highlighted peaks indicate the characteristic peaks for $MAPbBr_3$ perovskite material, representing formation of $MAPbBr_3$ NCs in composite material.

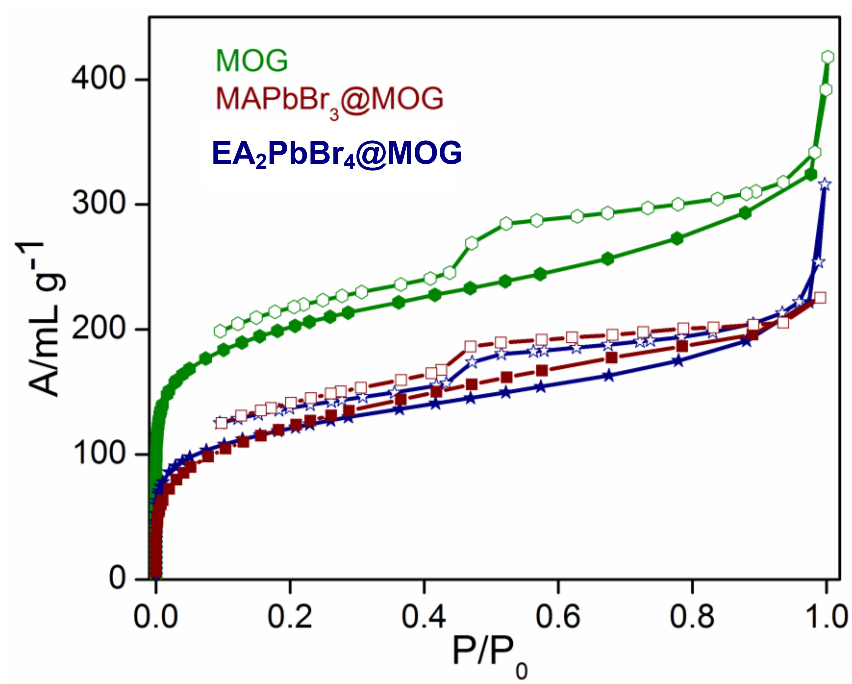

Figure S17. N_2 sorption study of MOG, $MAPbBr_3$@MOG and EA_2PbBr_4@MOG composites at 77 K.

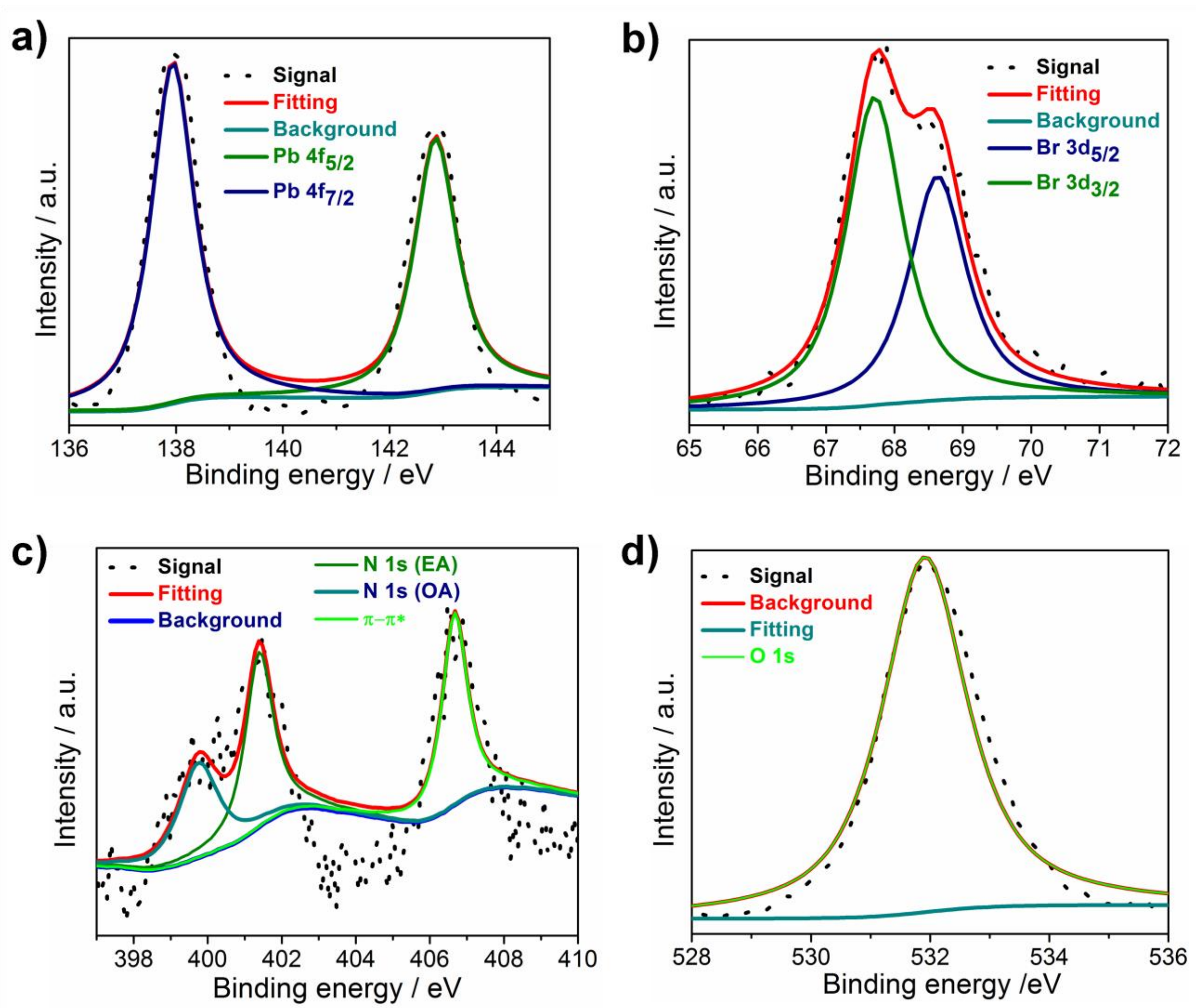

Figure S18. XPS spectra of EA_2PbBr_4@MOG. (a) Pb $4f_{5/2}$ and Pb $4f_{7/2}$; (b) Br $3d_{5/2}$ and Br 3d $_{3/2}$; (c) N 1s (EA), N 1s (OA) and π-π*; (d) O 1s.

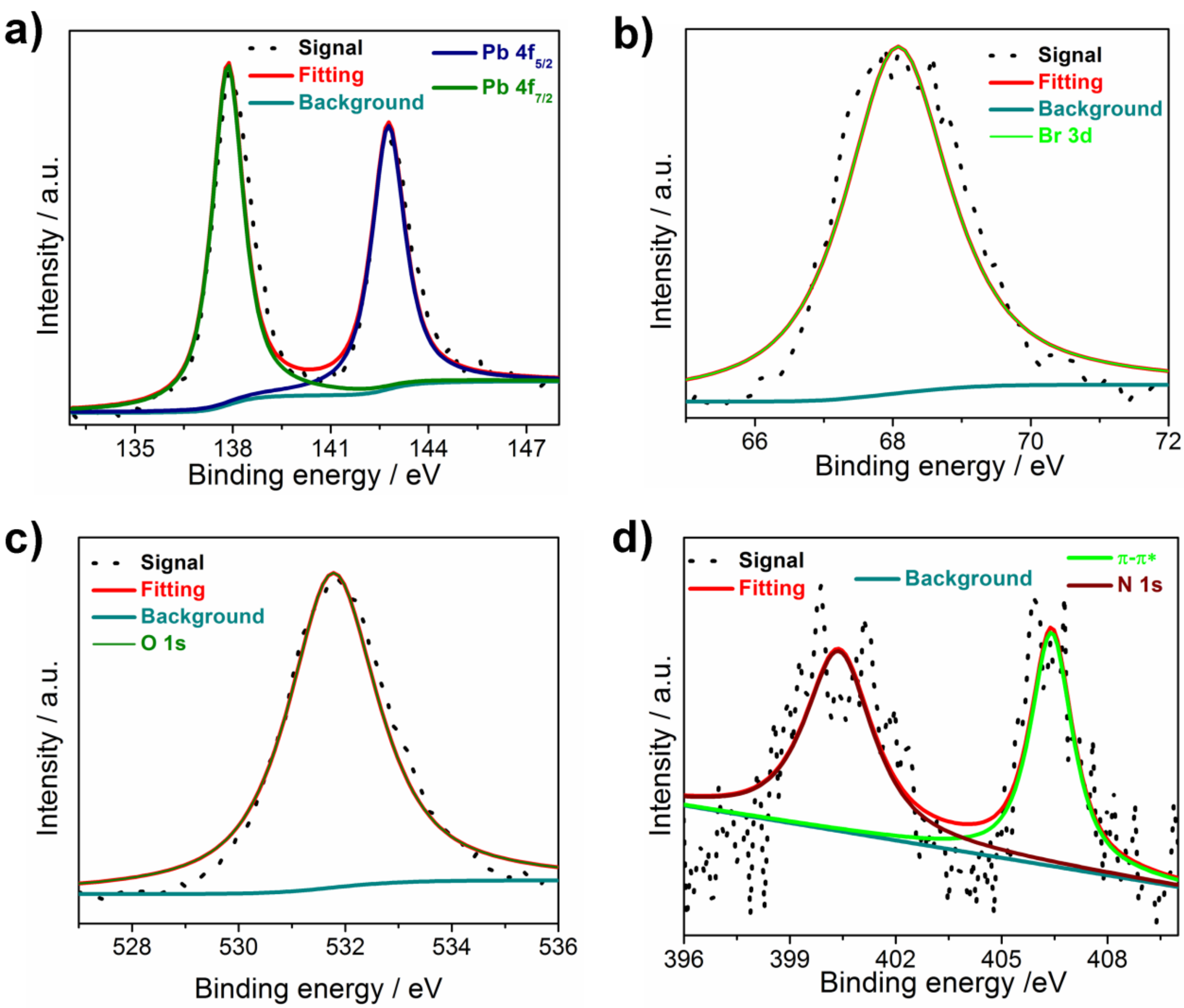

Figure S19. XPS spectra of $MAPbBr_3$@MOG. (a) Pb $4f_{5/2}$ and Pb $4f_{7/2}$; (b) Br $3d_{5/2}$ and Br $3d_{3/2}$; (d) N 1s (EA) and π-π*; (c) O 1s.

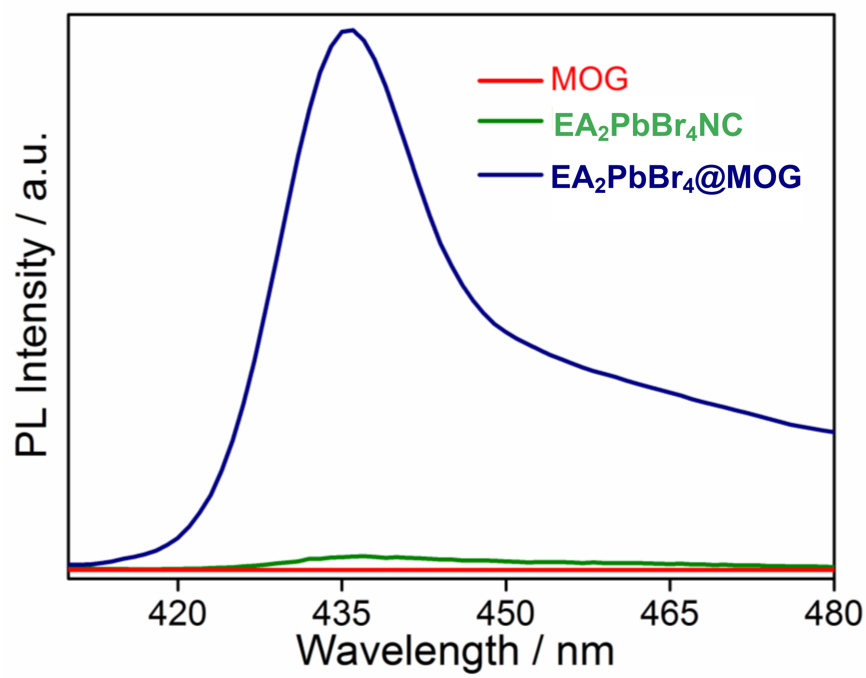

Figure S20. PL spectra of MOG, EA_2PbBr_4 NCs and EA_2PbBr_4@MOG composite.

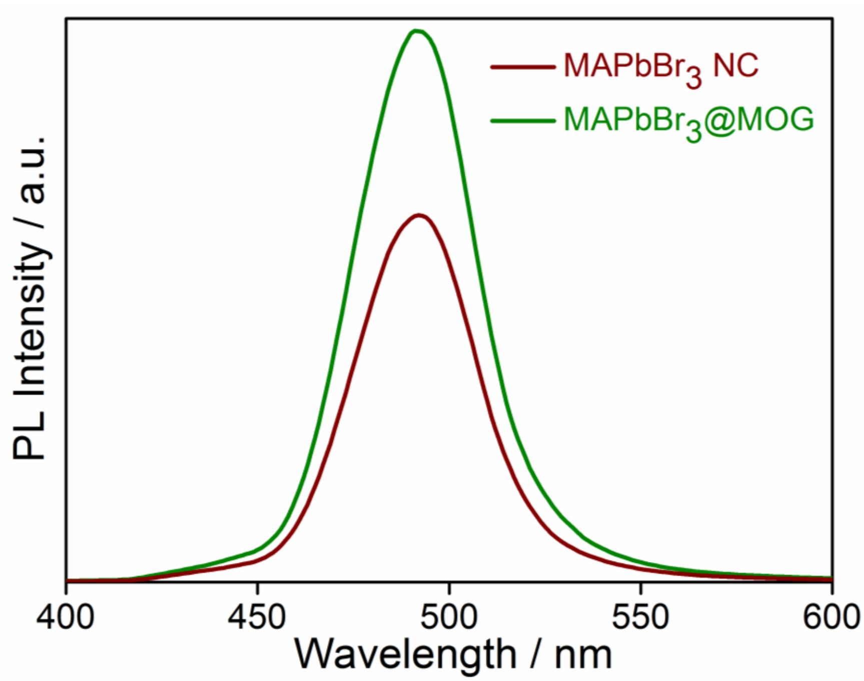

Figure S21. PL spectra of $MAPbBr_3$ NCs and $MAPbBr_3$@MOG composite.

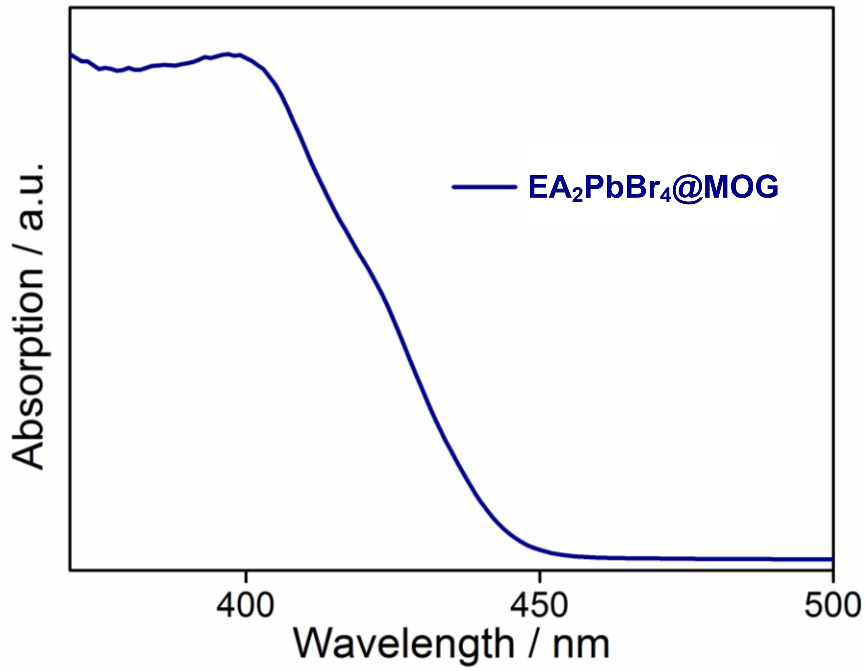

Figure S22. Solid state UV plot of EA_2PbBr_4@MOG composite material.

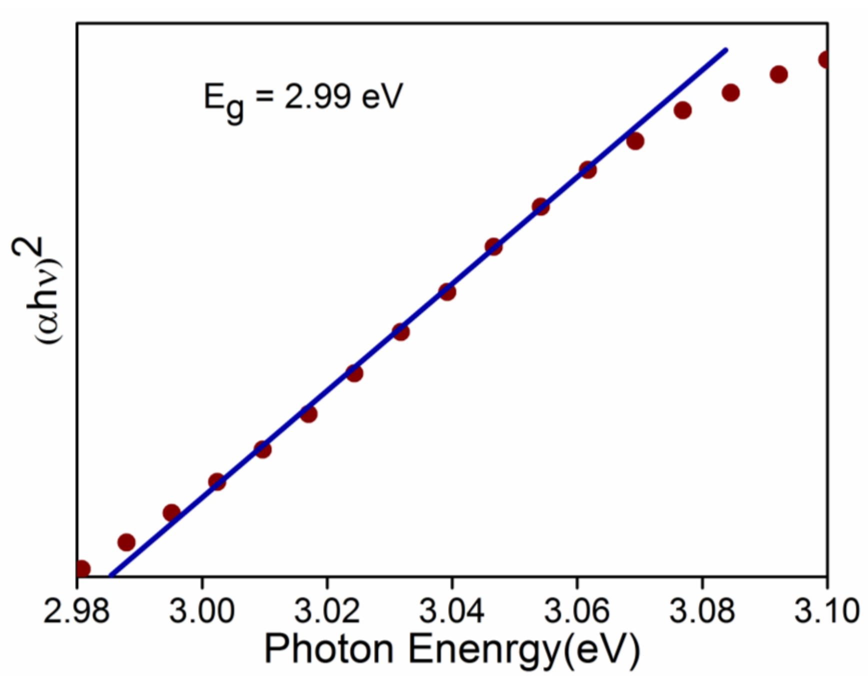

Figure S23. Tauc plot of EA_2PbBr_4@MOG composite material showing bandgap (E_g) ~ 2.99 eV.

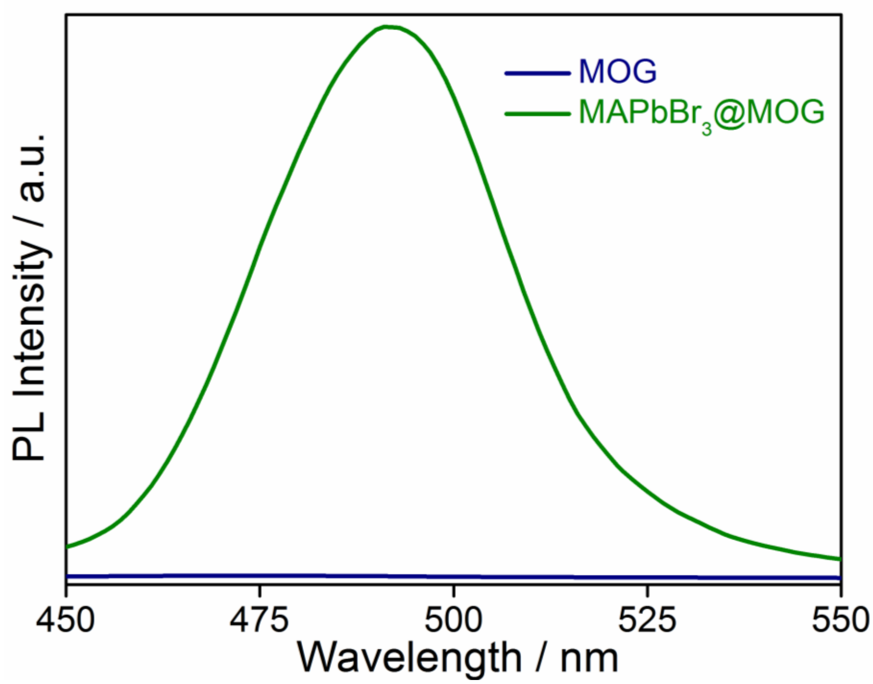

Figure S24. PL spectra of MOG and $MAPbBr_3$@MOG composite.

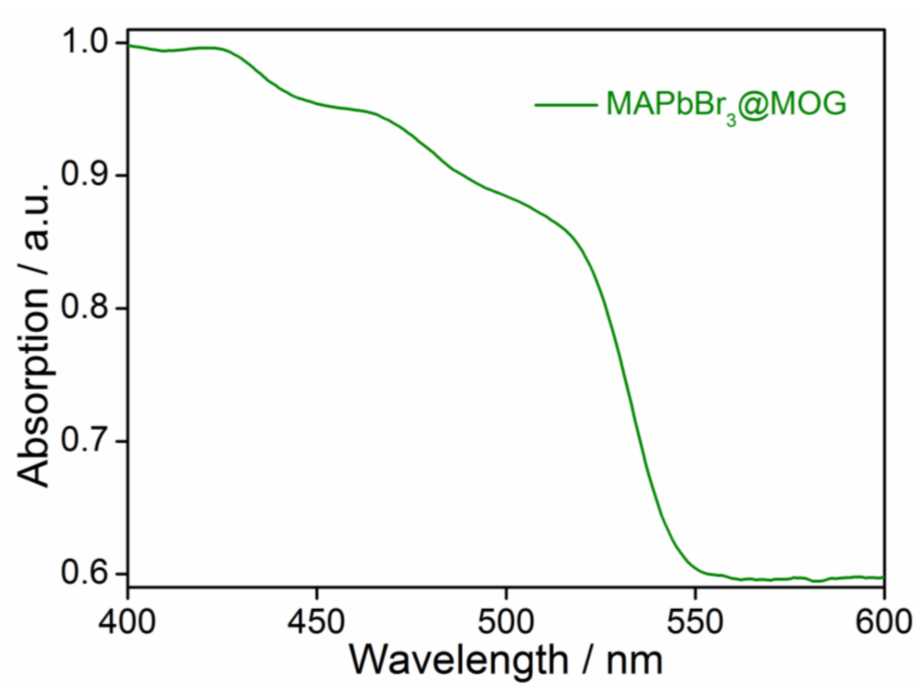

Figure S25. Solid state UV plot of $MAPbBr_3$@MOG composite material.

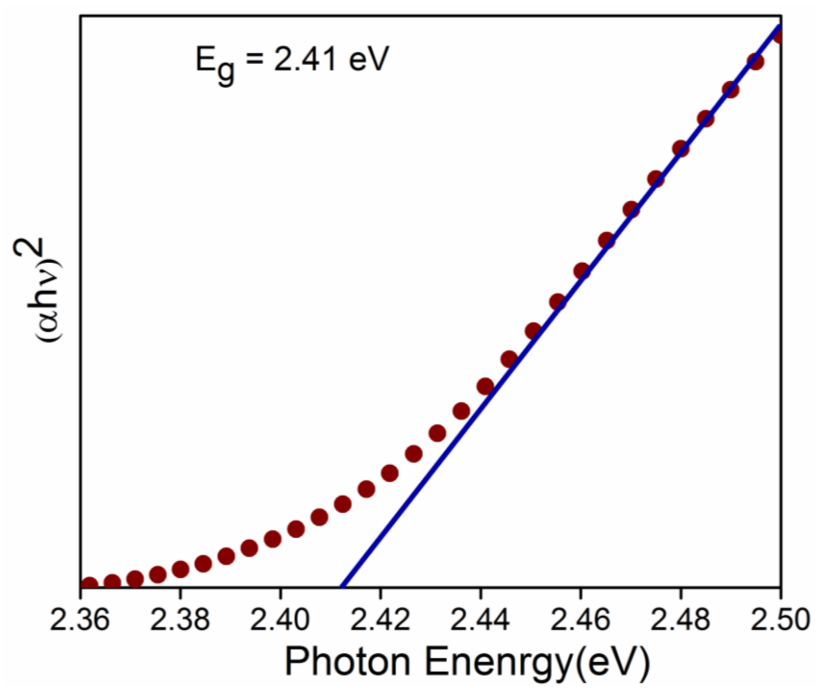

Figure S26. Tauc plot of $MAPbBr_3$@MOG composite showing bandgap (E_g) ~ 2.41 eV.

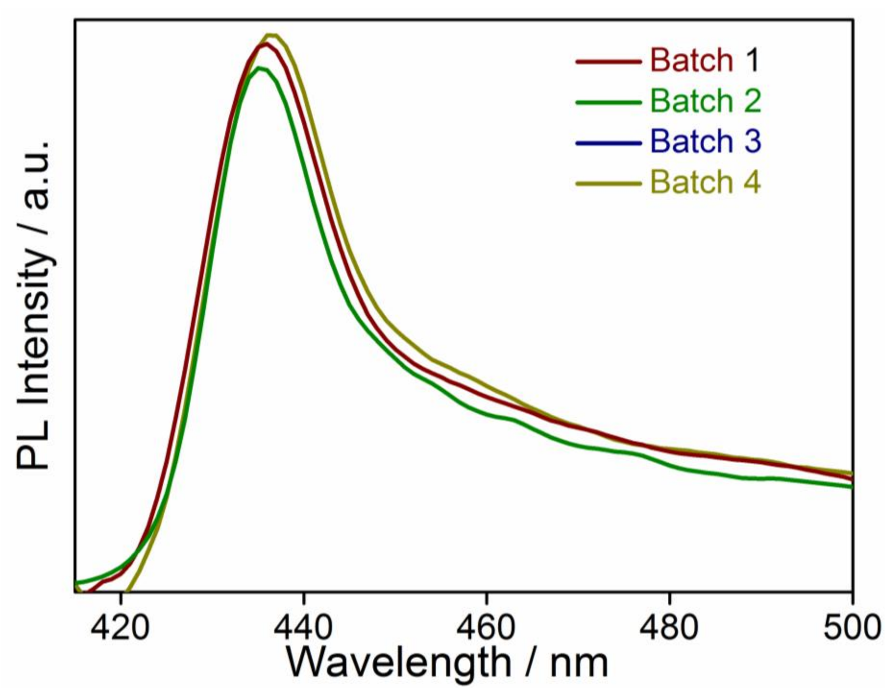

Figure S27. PL spectra of different batches of EA_2PbBr_4@MOG composite.

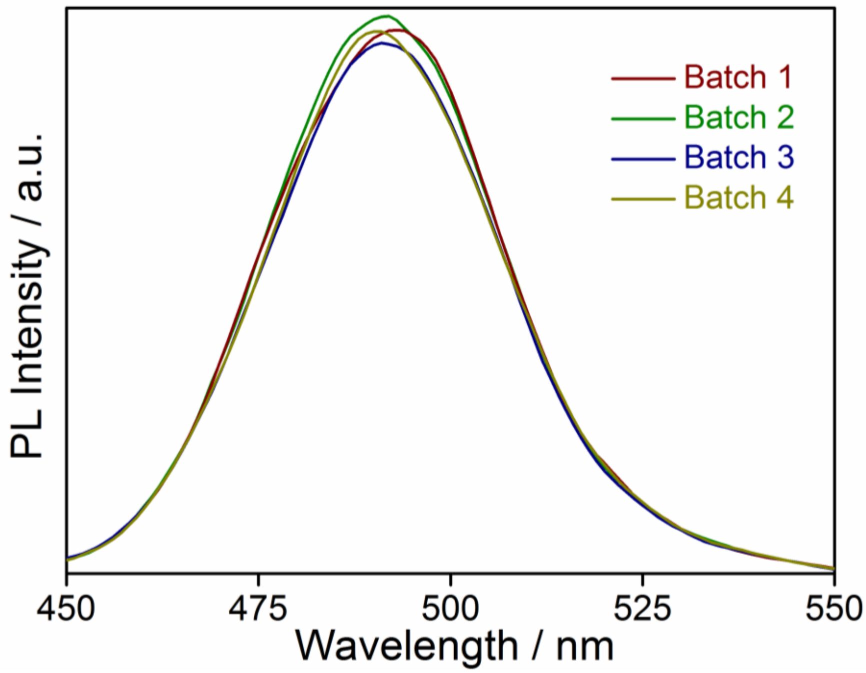

Figure S28. PL spectra of different batches of $MAPbBr_3$@MOG composite.

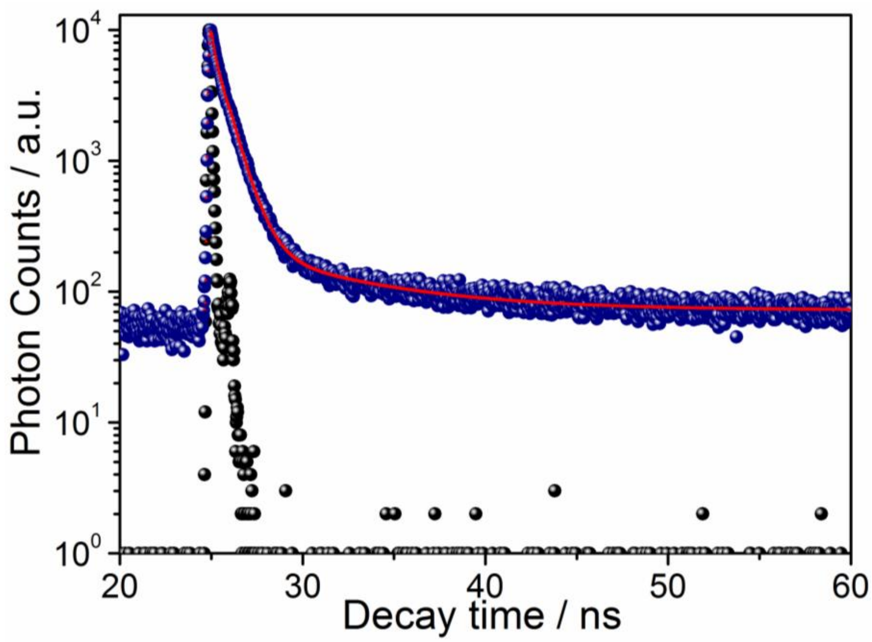

Figure S29. Time resolved PL spectra of EA_2PbBr_4 NCs.

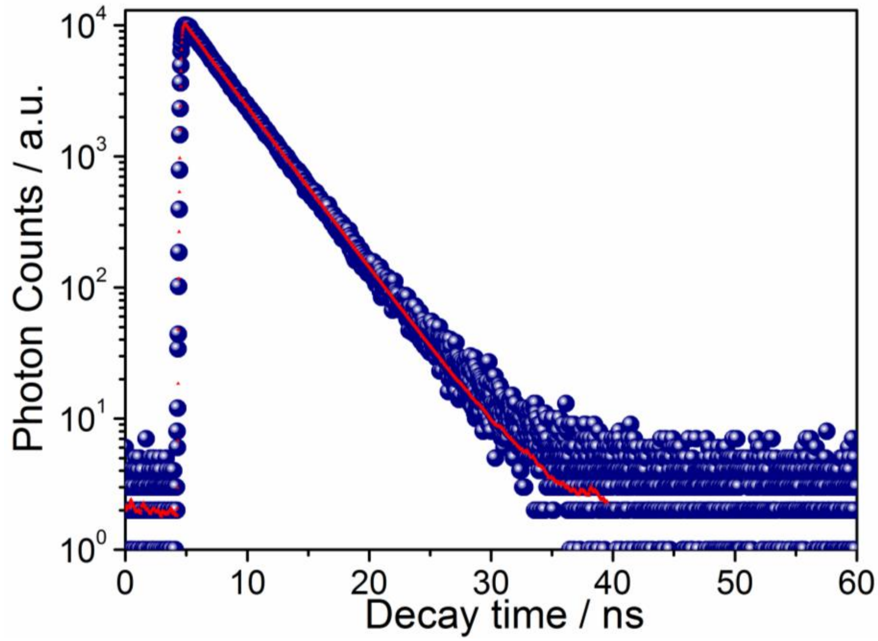

Figure S30. Time resolved PL spectra of EA_2PbBr_4@MOG nanocomposite. The average lifetime of composite larger than naked perovskite indicating confinement of EA_2PbBr_4 NCs inside MOG matrix.

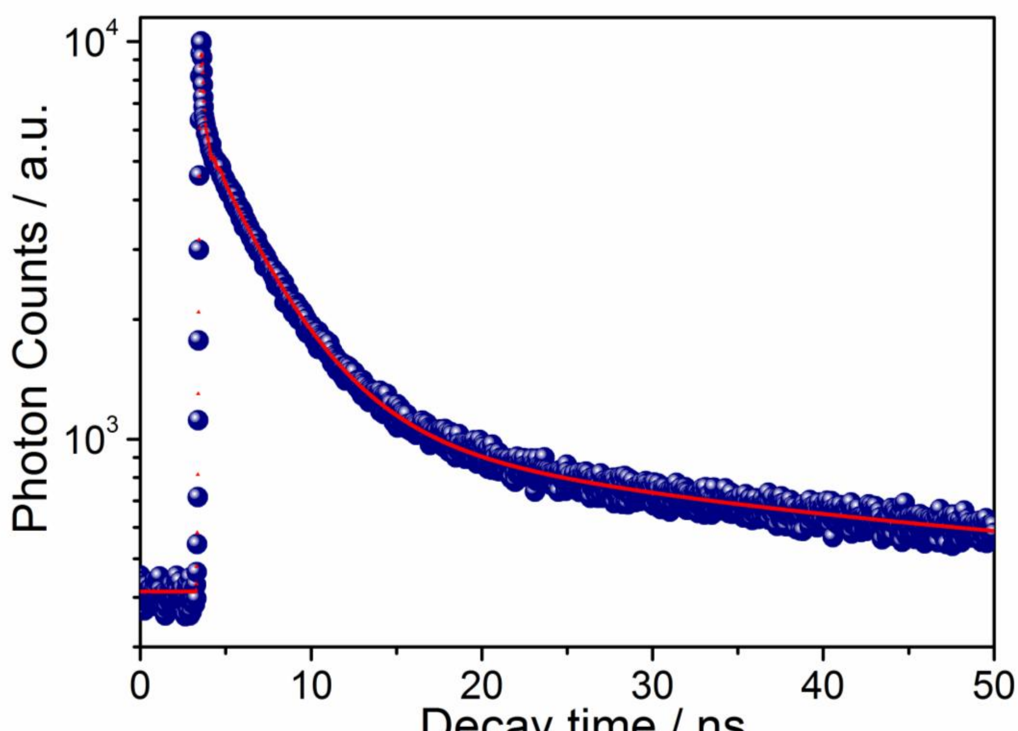

Figure S31. Time resolved PL spectra of $MAPbBr_3$@MOG nanocomposite.

Table S3. PL Decay parameters of EA_2PbBr_4 NCs and EA_2PbBr_4@MOG composite.

Compounds	τ_1(ns)	A_1	τ_2(ns)	A_2	χ^2	τ_{avg}(ns)	K_r(ns)	K_{nr}(ns)	K_r:K_{nr}
EA_2PbBr_4NC	0.10	0.56	0.80	0.44	1.16	0.71	0.03	1.39	0.02
EA_2PbBr_4@MOG	0.32	0.67	3.53	0.33	1.12	3.03	0.18	0.16	1.13

Table S4. PL Decay parameters of EA_2PbBr_4@MOG and $MAPbBr_3$@MOG composites.

Compounds	τ_1(ns)	A_1	τ_2(ns)	A_2	τ_3(ns)	A_3	χ^2	τ_{avg}(ns)
EA_2PbBr_4@MOG	0.32	0.67	3.53	0.33	-	-	1.12	3.40
$MAPbBr_3$@MOG	3.25	0.44	10.30	0.35	40.55	0.21	1.07	22.41

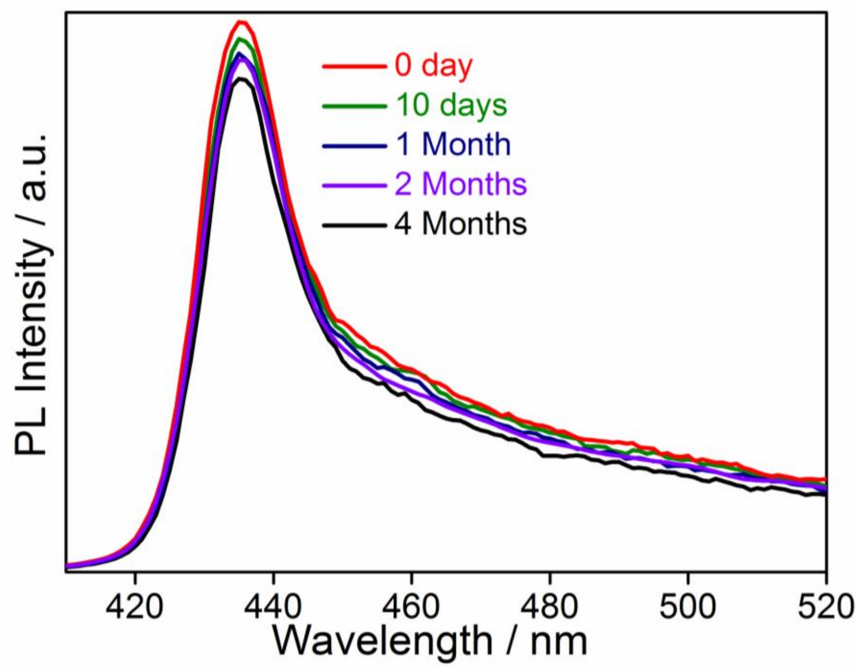

Figure S32. Change in PL intensity of EA_2PbBr_4@MOG composite with time in open air for 120 days.

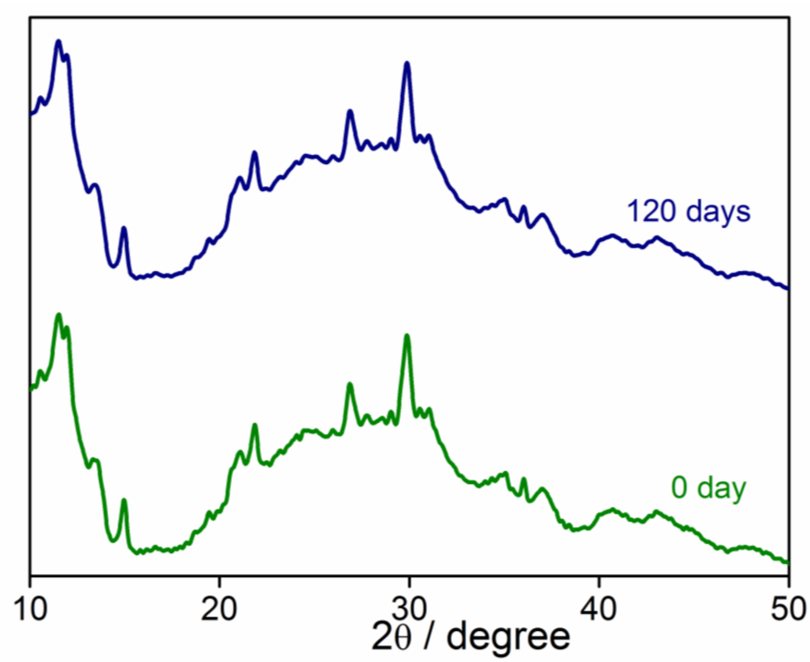

Figure S33. PXRD patterns of EA_2PbBr_4@MOG before and after 120 days kept in open air at RT.

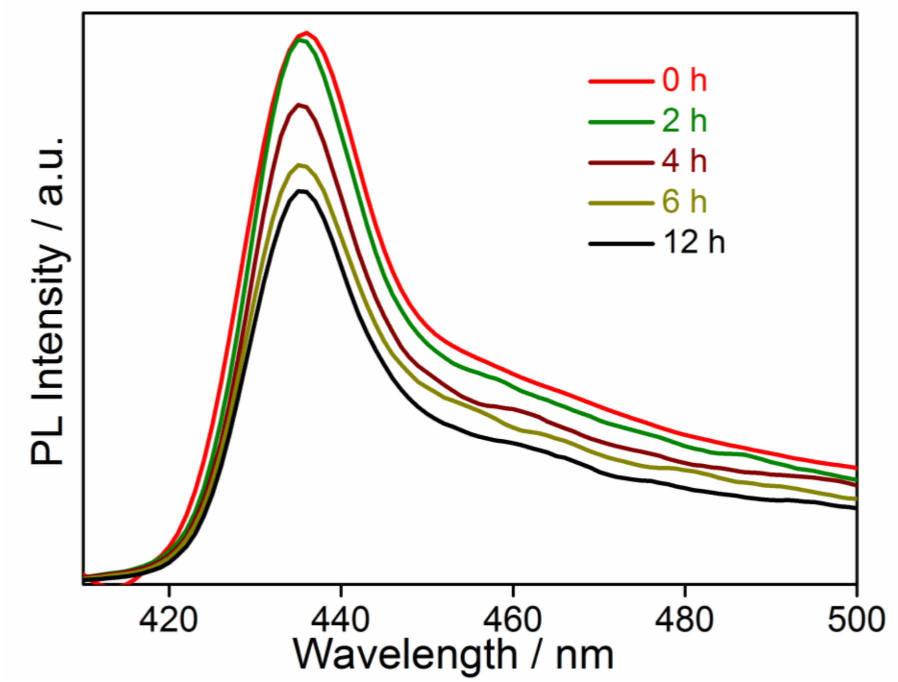

Figure S34. Time dependent PL spectra of EA_2PbBr_4@MOG composite after dipping in water for various time of interval.

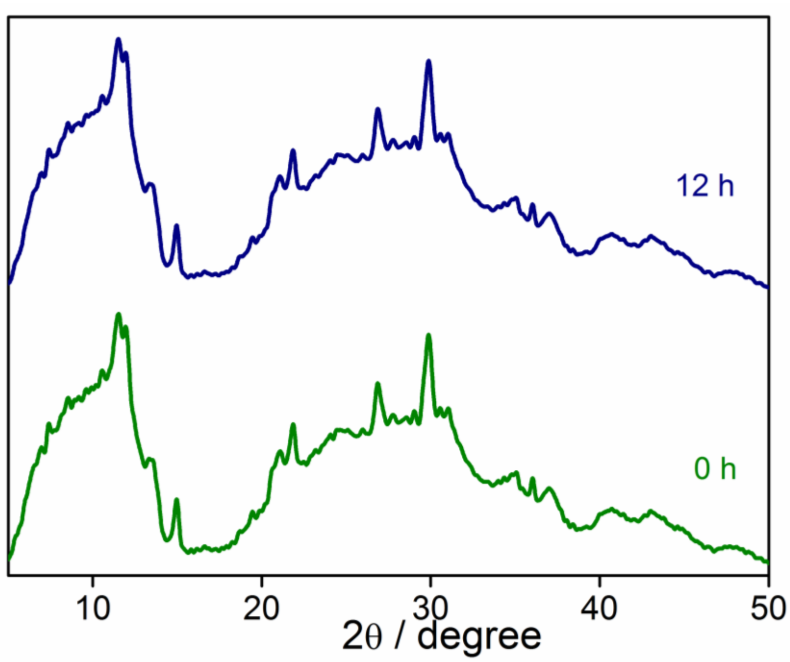

Figure S35. PXRD patterns of EA_2PbBr_4@MOG composite before and after 12 hours of water immersion.

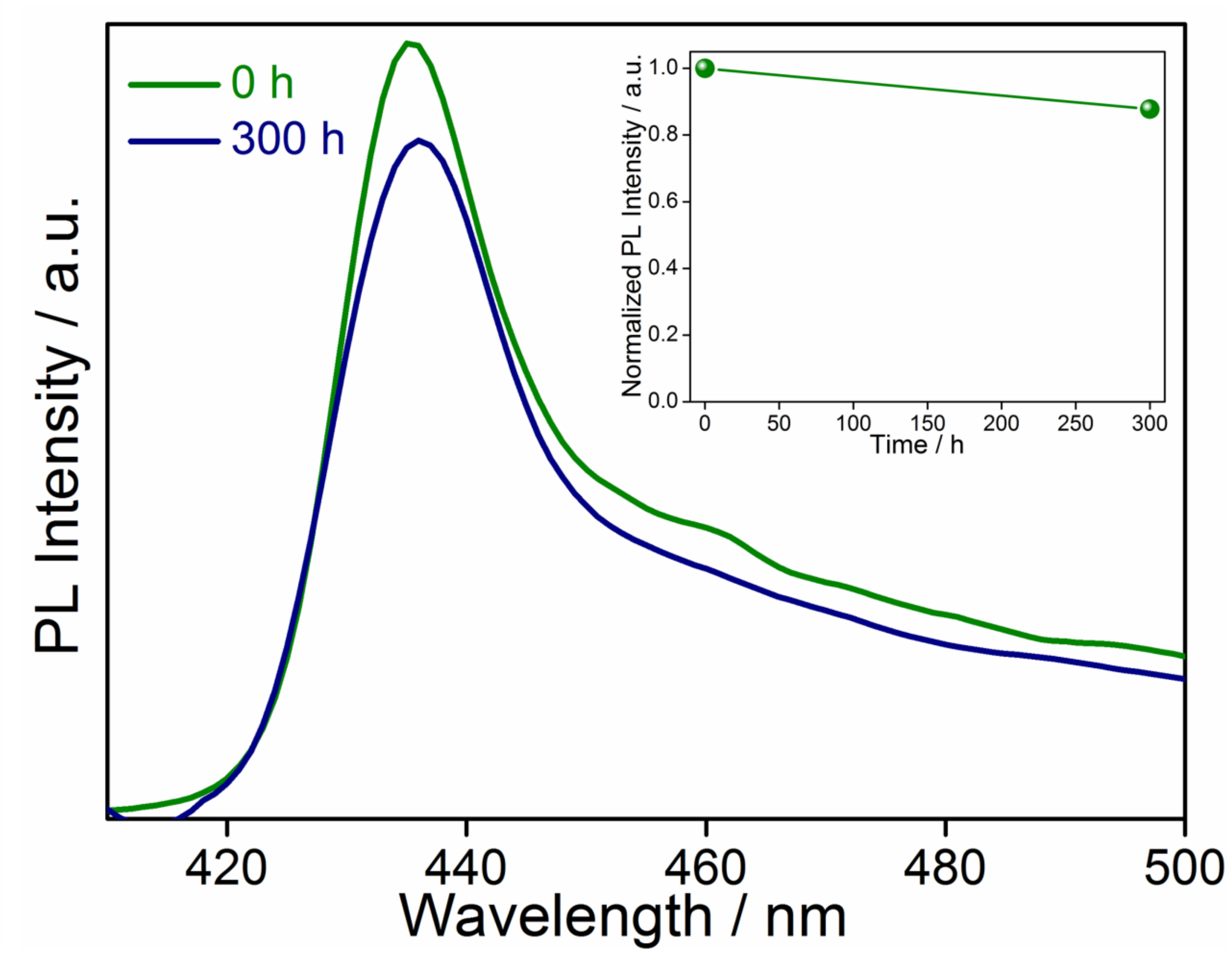

Figure S36. Time dependent PL spectra of EA_2PbBr_4@MOG, before and after keeping under UV light (365 nm) irradiation in dark condition upto 300 hours. Inset figure shows change in PL intensity of EA_2PbBr_4@MOG composite with time under UV light (365 nm) irradiation in dark condition.

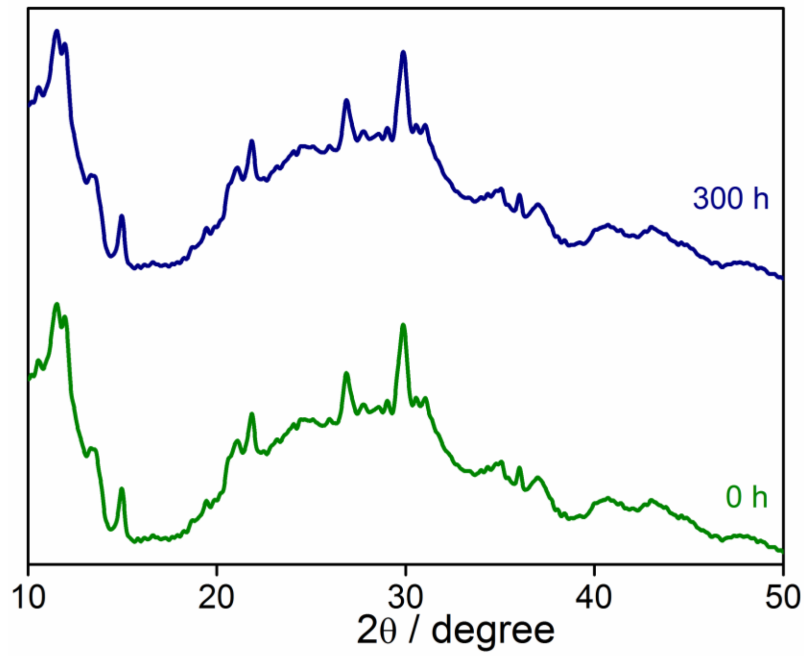

Figure S37. PXRD patterns of EA_2PbBr_4@MOG before and after irradiation of UV light (365 nm)**.**

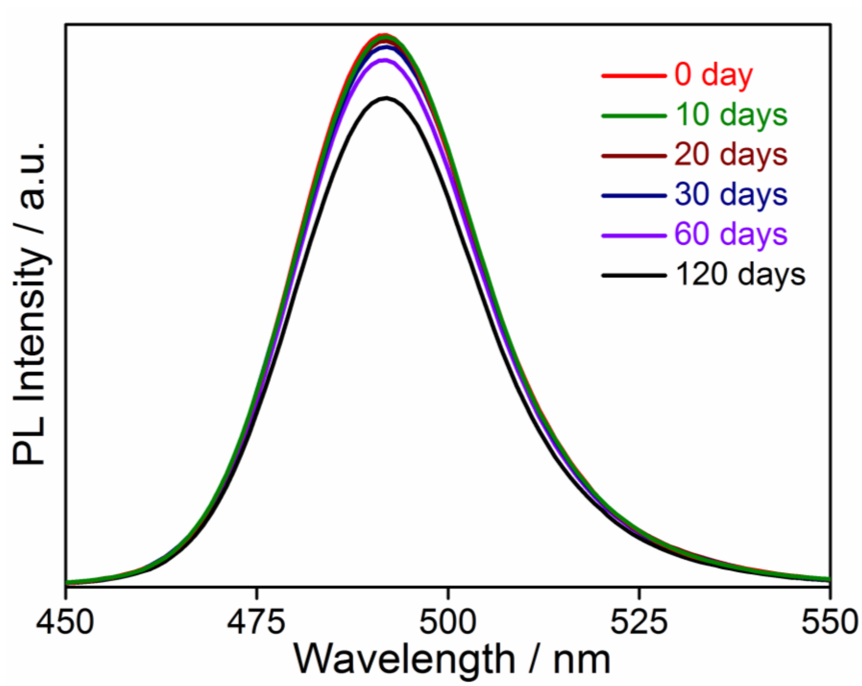

Figure S38. Time dependent PL spectra of $MAPbBr_3$@MOG composite stored under several months in open air**.**

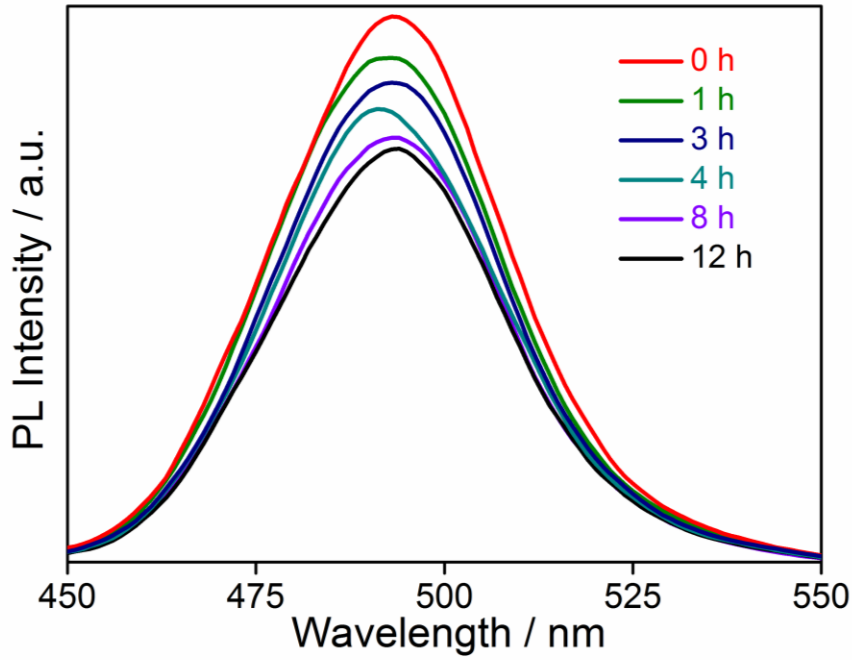

Figure S39. Time dependent PL spectra of $MAPbBr_3$@MOG in presence of water.

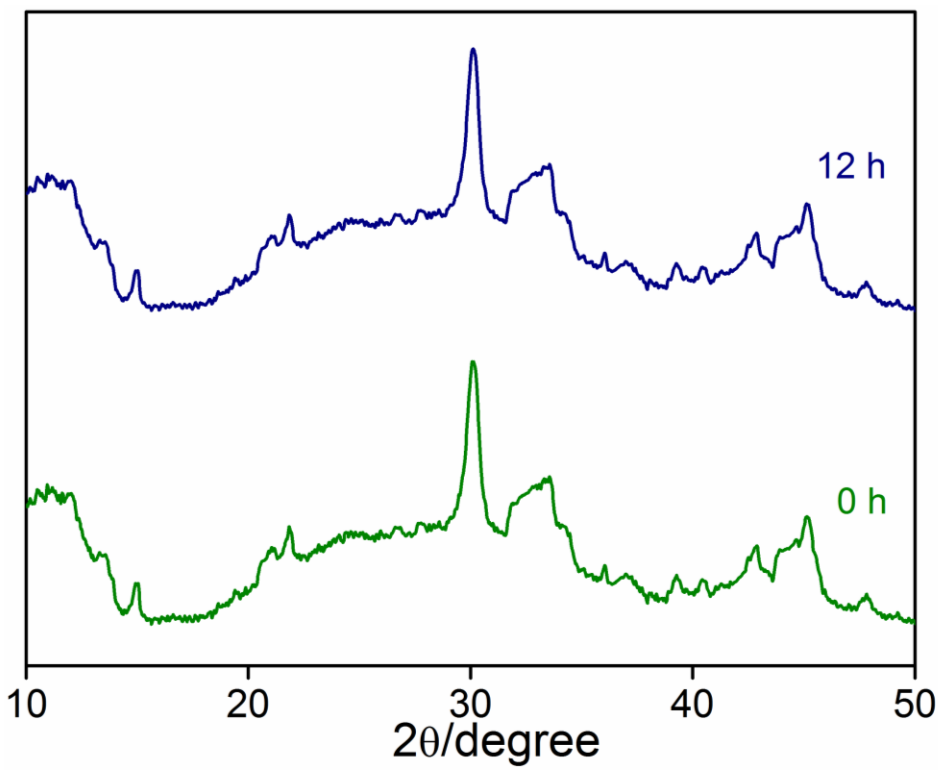

Figure S40. PXRD patterns of $MAPbBr_3$@MOG before and after immersion in water for 12 hours.

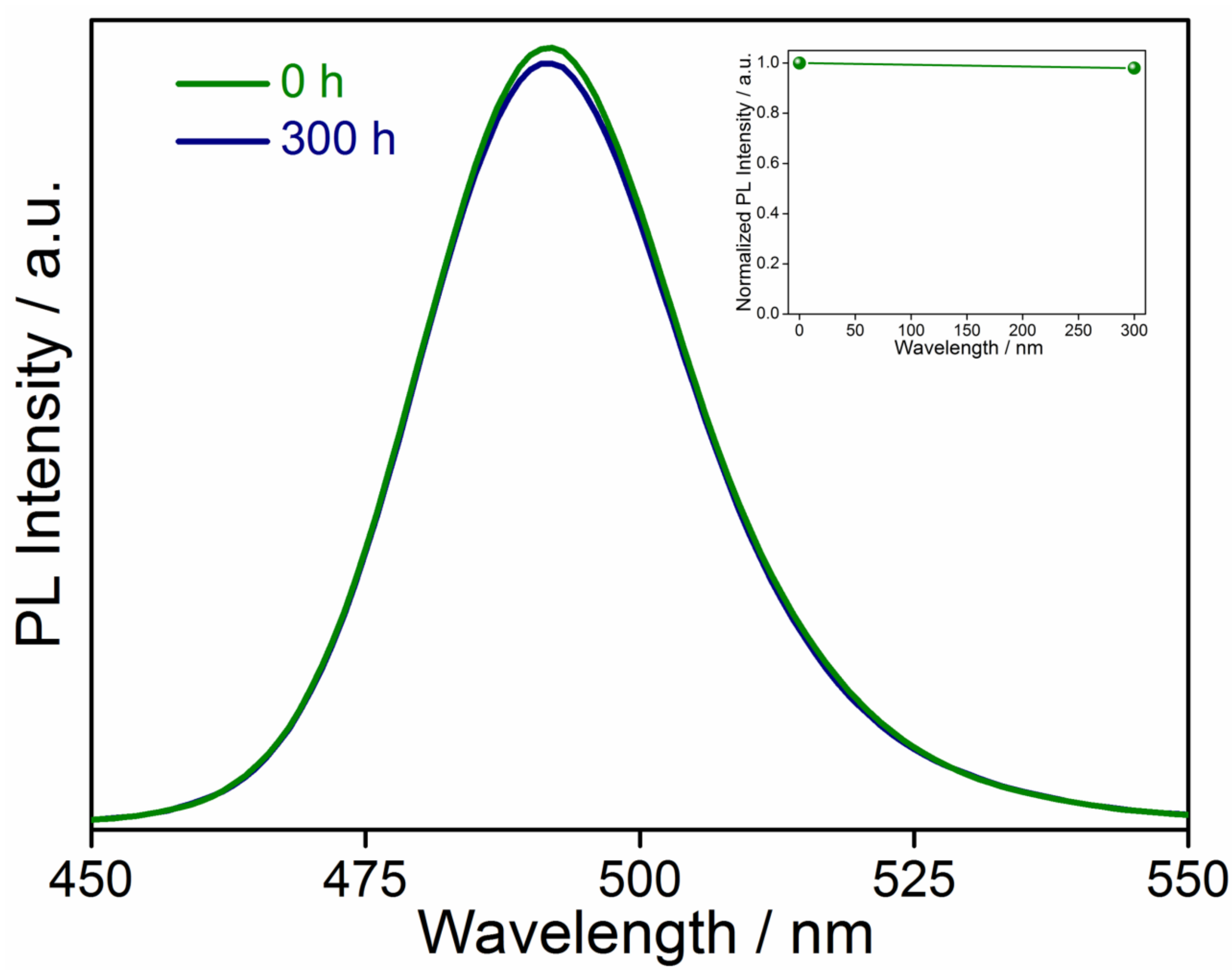

Figure S41. Time dependent PL spectra of $MAPbBr_3$@ZIF-8 composite under UV light (365 nm) irradiation for 300 h at dark condition. Inset figure shows change in PL intensity of $MAPbBr_3$@MOG composite with time under UV light.

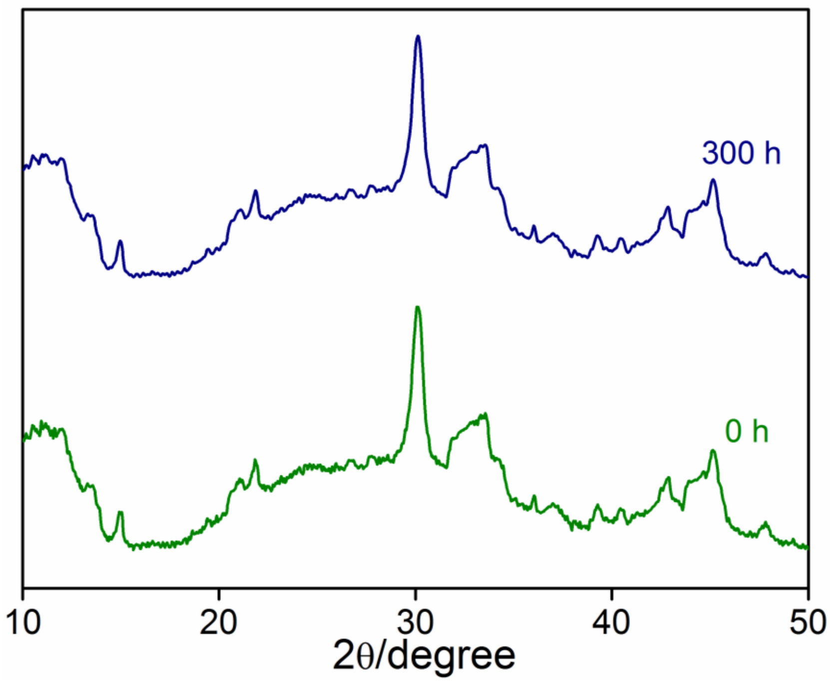

Figure S42. PXRD patterns of $MAPbBr_3$@MOG before and after exposure to UV light.

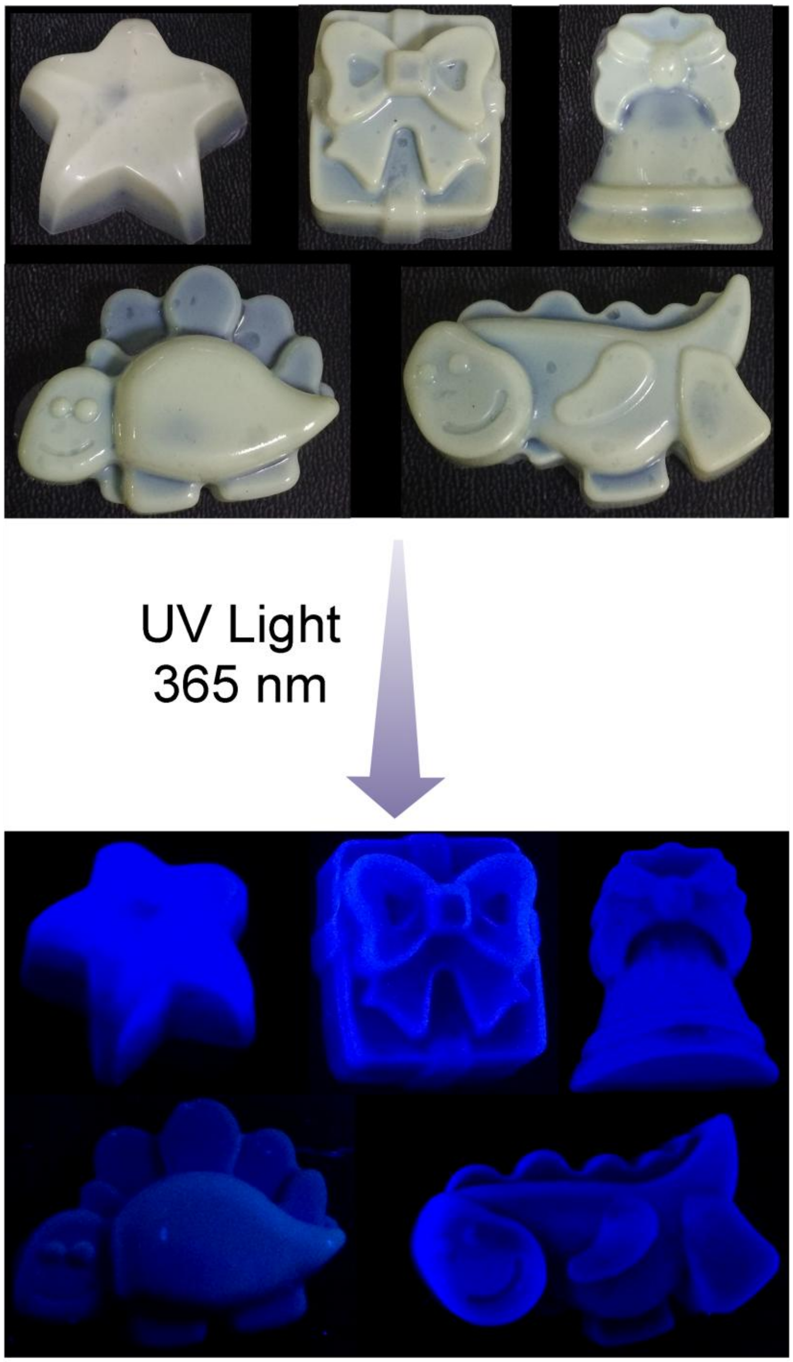

Figure S43. Photographs of various sculptures of EA_2PbBr_4@MOG at ambient condition and under 365 nm UV light.

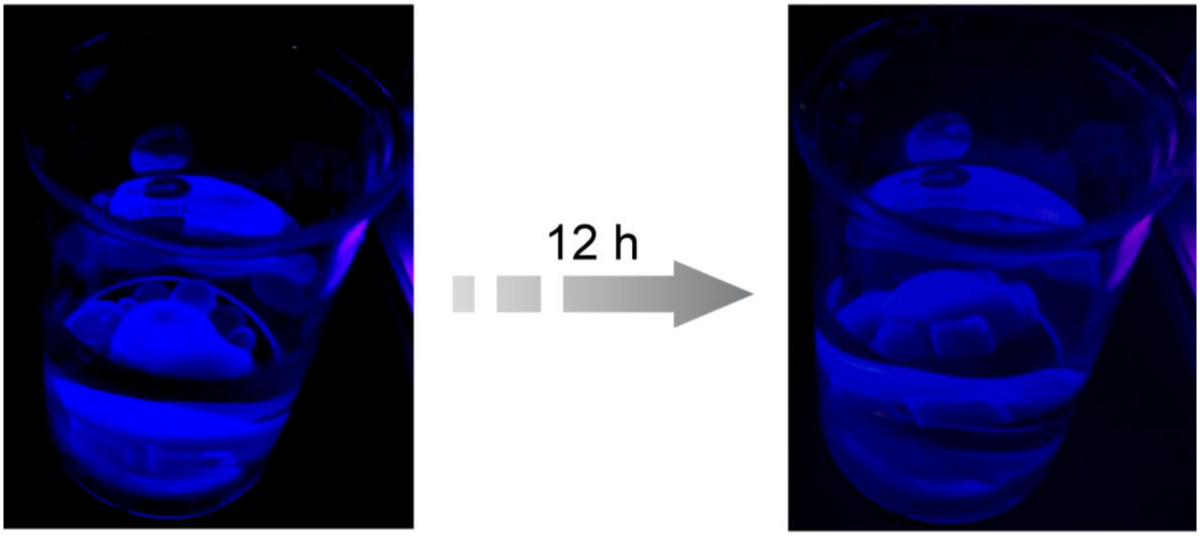

Figure S44. Photographs shows the water stability of sculpture fabricating from EA_2PbBr_4@MOG.

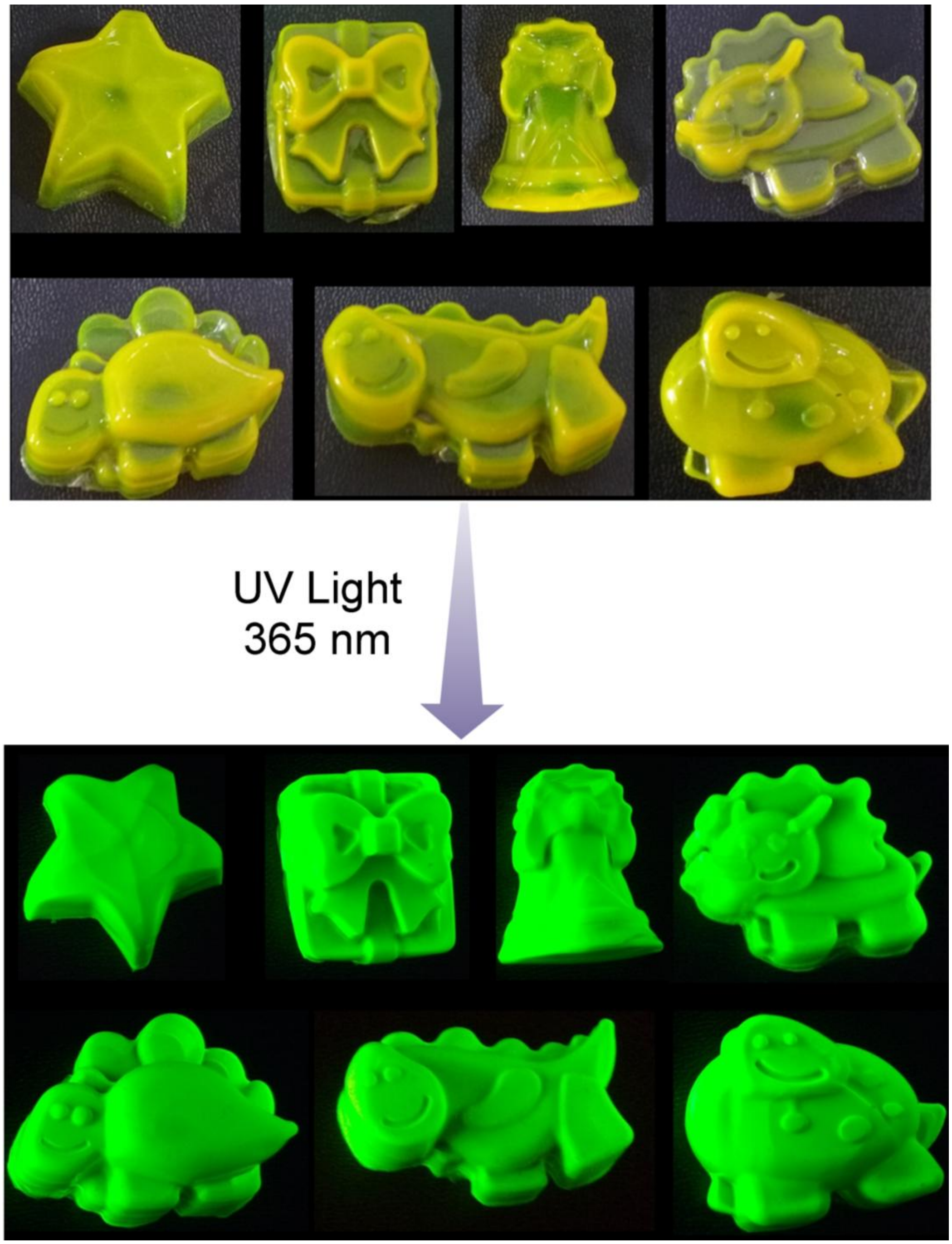

Figure S45. Photographs of various shaped sculptures synthesis from $MAPbBr_3$@MOG composites materials. The photographs shows the color at ambient condition and under UV light (365 nm).

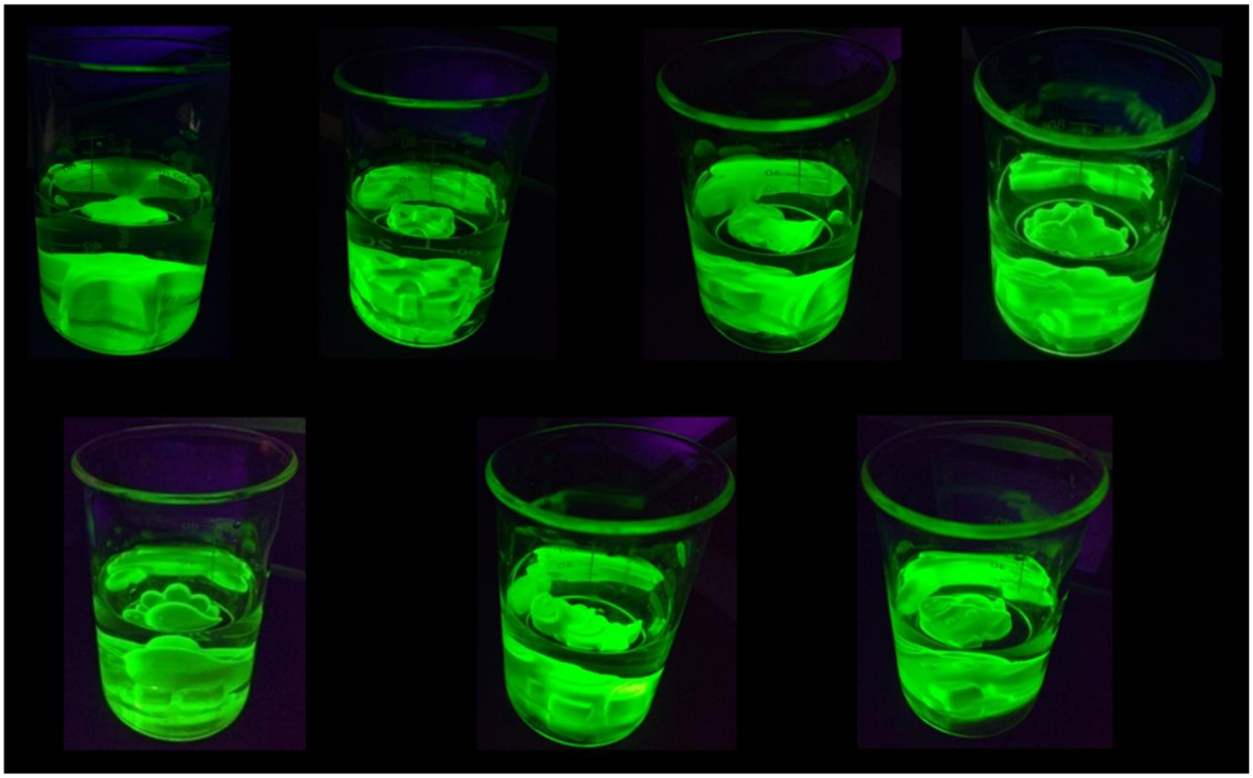

Figure S46. Different shaped sculptures were dipped in water under UV light (365 nm).

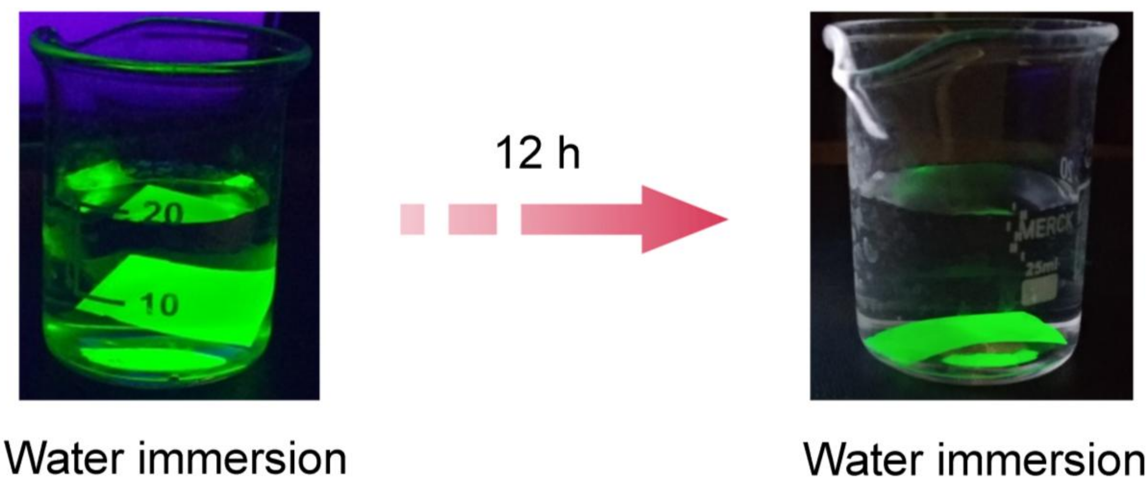

Figure S47. Photographs of water stability of thin film fabricated from $MAPbBr_3$@MOG composites under UV light (365 nm).

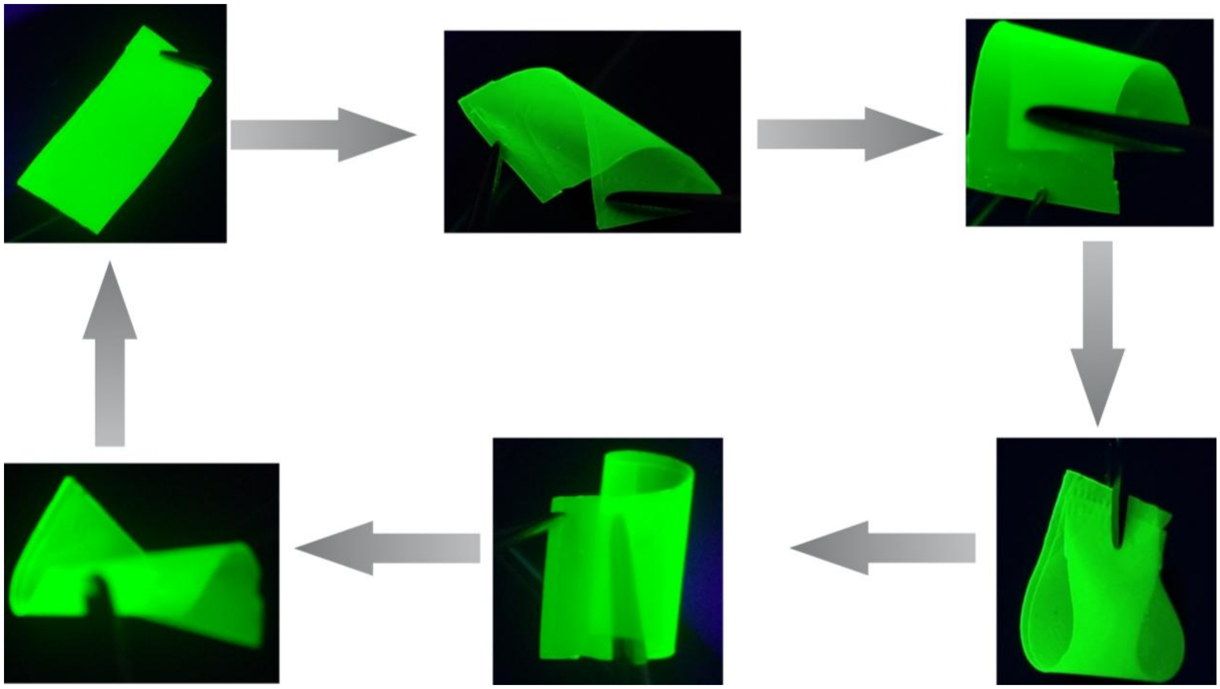

Figure S48. Photographs shows the thin film flexibility of $MAPbBr_3$@MOG composite under UV light (365 nm).

Table S5. Comparison of this work with other current related investigations of intense blue (λ_{max} <440 nm) hybrid perovskites.

System	PL Peak (nm)	PLQY (%)	FWHM (nm)	Air Stability	Photo Stability	Water Stability	Ref.
EA_2PbBr_4@MOG	436	53	18.4	4 months	300 h	12 h	This work
$(C_6H_5CH_2NH_3)$. $2PbBr_4$ exfoliated crystals	411	63 (Average)	20	-	-	-	[1]
$MAPbCl_3$	404	5	15	-	-	-	[2]
$MA_3Bi_2Br_9$	423	12	62	7 days	25 h	-	[3]
Cl-$MA_3Bi_2Br_9$	422	54.1	41	-	-	-	[4]
$(C_6H_5CH_2NH_3)$. $2PbBr_4$ nanoplates	403	53	11	-	30 min	-	[5]
$(PEA)_2PbBr_4$	409	46.5	10.6	-	-	-	[6]
$EAPbBr_3$	432	5	19.8	-	-	-	[7]

Abbreviations:

Phenylethylammonium (PEA).

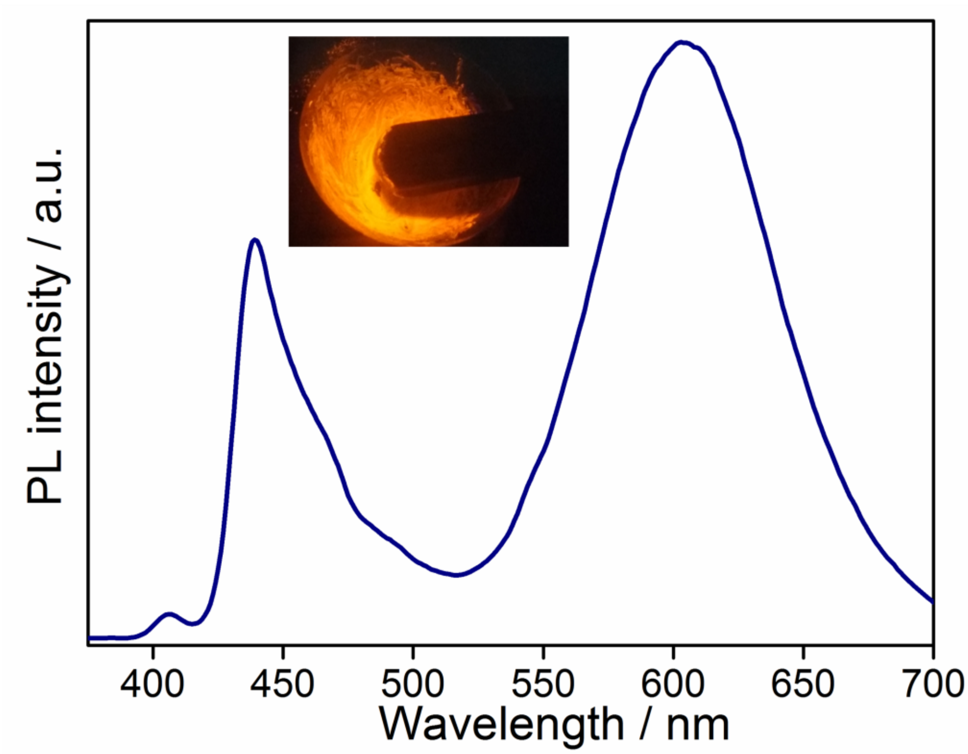

Figure S49. Emission spectra of Mn (II) doped EA_2PbBr_4. Inset photographs shows the color of Mn(II) doped EA_2PbBr_4 NCs under UV light (365 nm).

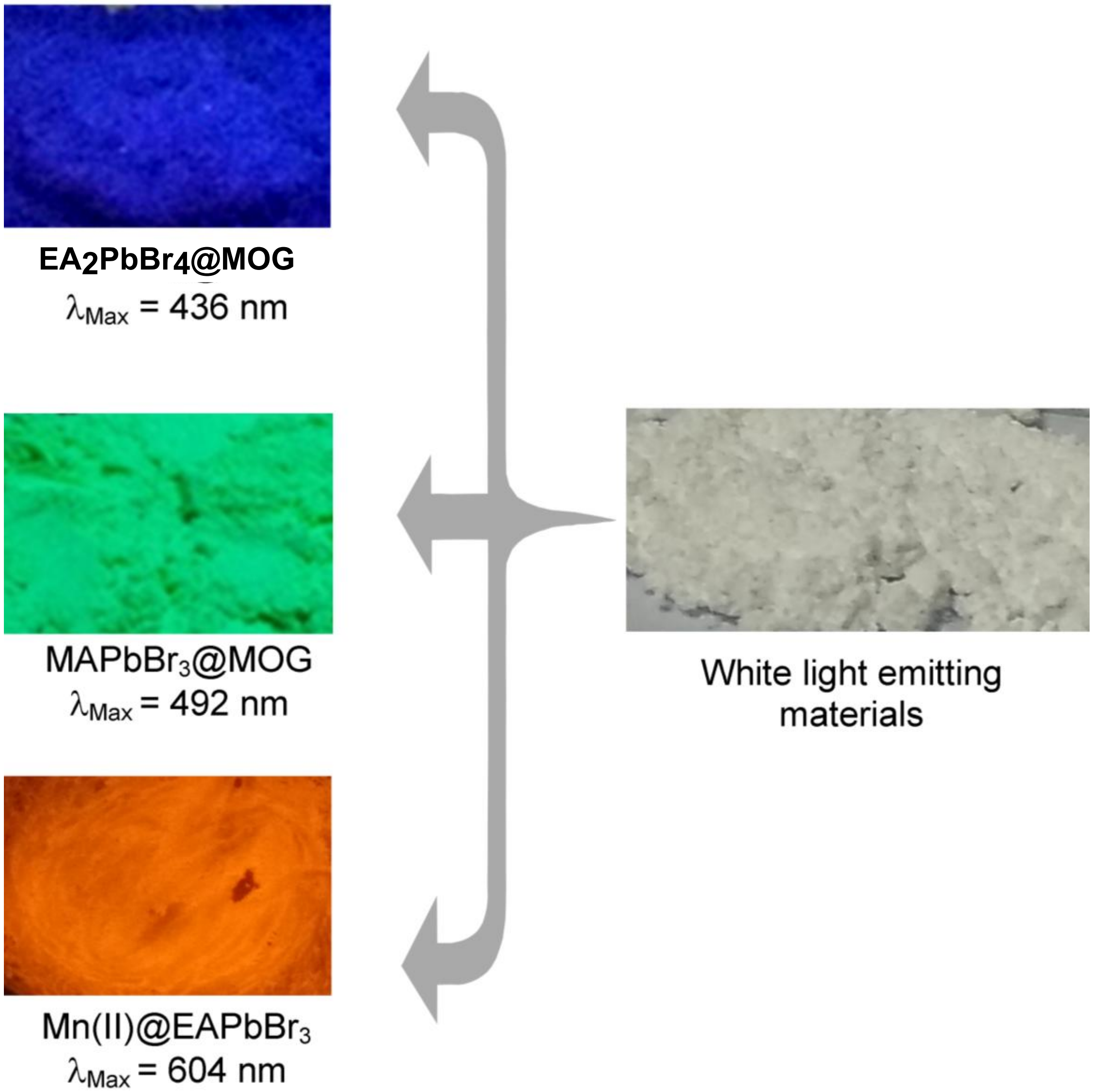

Figure S50. Proper mixing of blue emitting EA_2PbBr_4@MOG, green emitting $MAPbBr_3$@MOG and red emitting Mn(II)@EA_2PbBr_4 produce white light emitting material. The photographs of diffrent colored perovskite materials and white light emitting mateials are taken under UV light (365 nm).

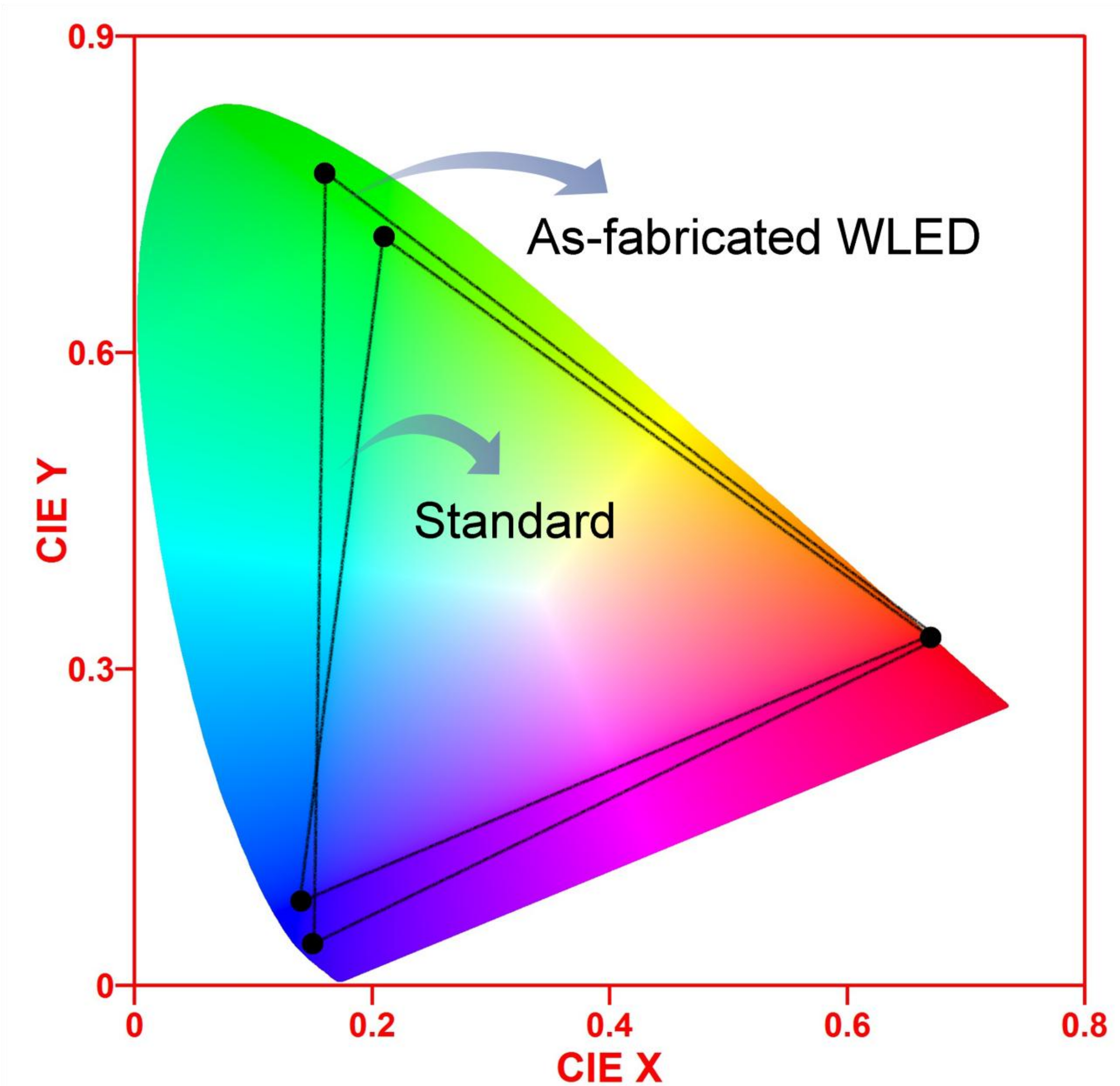

Figure S51. CIE color space coordinates of as-fabricated WLEDs showing the wide color gamut (144 % NTSC).

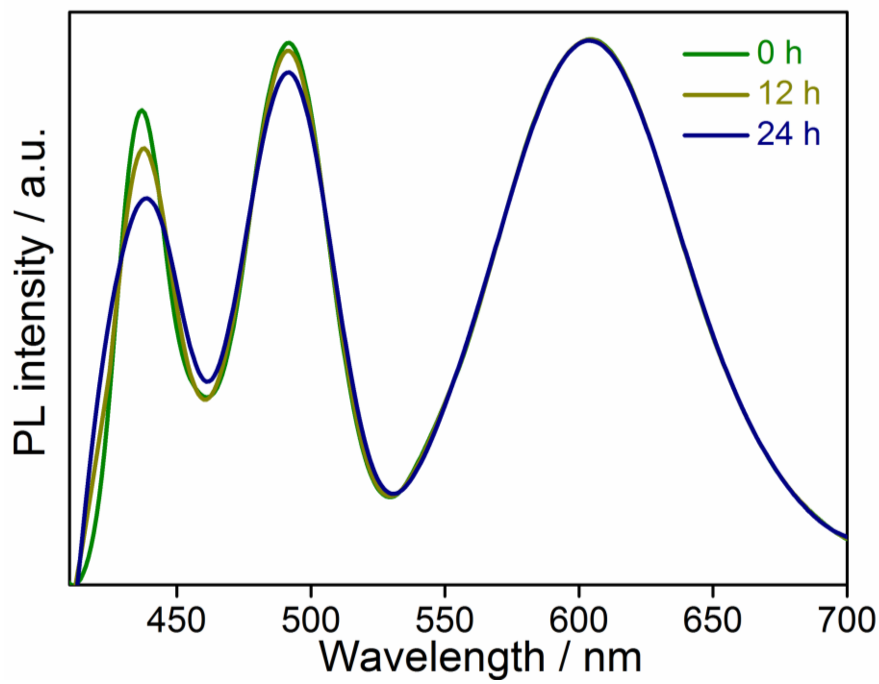

Figure S52. Time dependent PL spectra of as-fabricated WLEDs stored under open air**.**

References:

[1] X. Gong, O. Voznyy, A. Jain, W. Liu, R. Sabatini, Z. Piontkowski, G. Walters, G. Bappi, S. Nokhrin; O. Bushuyev, M. Yuan, R. Comin, D. McCamant, S. O. Kelley, E. H. Sargent, *Nat. Mater.*, 2018, **17**, 550-556.

[2] M. Imran, V. Caligiuri, M. Wang, L. Goldoni, M. Prato, R. Krahne, L. D. Trizio, L. Manna, *J. Am. Chem. Soc.*, 2018, **140**, 2656-2664.

[3] M. Leng, Z. Chen, Y. Yang, Z. Li, K. Zeng, K. Li, G. Niu, Y. He, Q. Zhou, J. Tang, *Angew. Chem. Int. Ed.*, 2016, **55**, 15012-15016.

[4] M. Leng, Y. Yang, Z. Chen, W. Gao, J. Zhang, G. Niu, D. Li, H. Song, J. Zhang, S. Jin, J. Tang, *Nano Lett*., 2018, **18**, 6076-6083.

[5] D. Liang, Y. Peng, Y. Fu, M. J. Shearer, J. Zhang, J. Zhai, Y. Zhang, R. J. Hamers, T. L. Andrew, S. Jin, *ACS Nano*, 2016, **10**, 6897-6904.

[6] S. Yang, W. Niu, A.-L. Wang, Z. Fan, B. Chen, C. Tan, Q. Lu, H. Zhang, *Angew. Chem. Int. Ed.*, 2017, **56**, 4252-4255.

[7] M. Mittal, A. Jana, S. Sarkar, P. Mahadevan, S. Sapra, *J. Phys. Chem. Lett.*, 2016, **7**, 3270-3277.